




# Constraining axion-like particles with the diffuse gamma-ray flux measured by the Large High Altitude Air Shower Observatory

Leonardo Mastrototaro<sup>1,2,a</sup> , Pierluca Carenza<sup>3,b</sup>, Marco Chianese<sup>4,5,c</sup>, Damiano F.G. Fiorillo<sup>4,5,6,d</sup>, Gennaro Miele<sup>4,5,7,e</sup>, Alessandro Mirizzi<sup>8,9,f</sup>, Daniele Montanino<sup>10,11,g</sup>

<sup>1</sup> Dipartimento di Fisica “E.R. Caianiello”, Università degli Studi di Salerno, Via Giovanni Paolo II, 132, 84084 Fisciano, SA, Italy

<sup>2</sup> INFN-Gruppo Collegato di Salerno-Sezione di Napoli, Via Giovanni Paolo II, 132, 84084 Fisciano, SA, Italy

<sup>3</sup> The Oskar Klein Centre, Department of Physics, Stockholm University, 106 91 Stockholm, Sweden

<sup>4</sup> Dipartimento di Fisica “Ettore Pancini”, Università degli studi di Napoli “Federico II”, Complesso Universitario Monte S. Angelo, 80126 Naples, Italy

<sup>5</sup> INFN-Sezione di Napoli, Complesso Universitario Monte S. Angelo, 80126 Naples, Italy

<sup>6</sup> Niels Bohr International Academy, Niels Bohr Institute, University of Copenhagen, Copenhagen, Denmark

<sup>7</sup> Scuola Superiore Meridionale, Università degli studi di Napoli “Federico II”, Largo San Marcellino 10, 80138 Naples, Italy

<sup>8</sup> Dipartimento Interateneo di Fisica “Michelangelo Merlin”, Via Amendola 173, 70126 Bari, Italy

<sup>9</sup> Istituto Nazionale di Fisica Nucleare-Sezione di Bari, Via Orabona 4, 70126 Bari, Italy

<sup>10</sup> Dipartimento di Matematica e Fisica “Ennio De Giorgi”, Università del Salento, Via Arnesano, 73100 Lecce, Italy

<sup>11</sup> Istituto Nazionale di Fisica Nucleare-Sezione di Lecce, Via Arnesano, 73100 Lecce, Italy

Received: 18 August 2022 / Accepted: 29 October 2022 / Published online: 11 November 2022  
© The Author(s) 2022

**Abstract** The detection of very high-energy neutrinos by IceCube experiment supports the existence of a comparable gamma-ray counterpart from the same cosmic accelerators. Under the likely assumption that the sources of these particles are of extragalactic origin, the emitted photon flux would be significantly absorbed during its propagation over cosmic distances. However, in the presence of photon mixing with ultra-light axion-like-particles (ALPs), this expectation would be strongly modified. Notably, photon-ALP conversions in the host galaxy would produce an ALP flux which propagates unimpeded in the extragalactic space. Then, the back-conversion of ALPs in the Galactic magnetic field leads to a diffuse high-energy photon flux. In this context, the recent detection of the diffuse high-energy photon flux by the Large High Altitude Air Shower Observatory (LHAASO) allows us to exclude at the 95% CL an ALP-photon coupling  $g_{a\gamma} \gtrsim 3.9\text{--}7.8 \times 10^{-11} \text{ GeV}^{-1}$  for  $m_a \lesssim 4 \times 10^{-7} \text{ eV}$ , depending on the assumptions on the magnetic fields and on the original gamma-ray spectrum. This new bound is comple-

mentary with other ALP constraints from very-high-energy gamma-ray experiments and sensitivities of future experiments.

## 1 Introduction

Ultra-light Axion-Like-Particles (ALPs) often appear in various Standard Model extensions, including effective models derived from string theory [1–3], or in the context of “relaxion” models [4]. Similarly to the QCD axion, ALPs can also be thought as pseudo-Nambu-Goldstone bosons of broken, approximate symmetries, (see e.g. Sec. 6.7 of Ref. [5] for a recent review). A minimal model of ALPs accounts for their electromagnetic coupling through the Lagrangian term [6]

$$\mathcal{L}_{a\gamma} = -\frac{1}{4} g_{a\gamma} F_{\mu\nu} \tilde{F}^{\mu\nu} a = g_{a\gamma} \mathbf{E} \cdot \mathbf{B} a, \quad (1)$$

where  $g_{a\gamma}$  is the ALP-photon coupling constant,  $F_{\mu\nu}$  is the electromagnetic field tensor and  $\tilde{F}_{\mu\nu} = \frac{1}{2} \epsilon_{\mu\nu\rho\sigma} F^{\rho\sigma}$  is its dual, and the ALP,  $a$ , is assumed to have a mass  $m_a$ . The coupling in Eq. (1) induces a mixing between ALPs and photons in a background electromagnetic field, leading the two states to oscillate into one another [6,7]. This conversion phenomenon is the basis for the majority of the experimental and observational ALP searches (see, e.g., Refs. [8–11])

<sup>a</sup> e-mail: [lmastrototaro@unisa.it](mailto:lmastrototaro@unisa.it) (corresponding author)

<sup>b</sup> e-mail: [pierluca.carenza@fysik.su.se](mailto:pierluca.carenza@fysik.su.se)

<sup>c</sup> e-mail: [chianese@na.infn.it](mailto:chianese@na.infn.it)

<sup>d</sup> e-mail: [damiano.fiorillo@nbi.ku.dk](mailto:damiano.fiorillo@nbi.ku.dk)

<sup>e</sup> e-mail: [miele@na.infn.it](mailto:miele@na.infn.it)

<sup>f</sup> e-mail: [alessandro.mirizzi@ba.infn.it](mailto:alessandro.mirizzi@ba.infn.it)

<sup>g</sup> e-mail: [daniele.montanino@le.infn.it](mailto:daniele.montanino@le.infn.it)

for recent reviews). Conversions of very-high-energy (VHE) cosmic photons into ultra-light ALPs (with  $m_a \lesssim 10^{-7}$  eV) in cosmic magnetic fields of Galactic or extragalactic origin have been proposed as an intriguing possibility to perform ALP searches with gamma-ray telescopes (see, e.g., Refs. [12–17] for seminal papers). VHE photon-ALP conversions would imprint peculiar modulations in astrophysical spectra from faraway sources, such as blazars, active galactic nuclei, pulsars and galaxy clusters, see, e.g., Refs. [18–37] for an incomplete list of studies that pointed out intriguing hints and bounds on ALP parameter space (see also Ref. [38] for a recent review).

The production of VHE gamma-rays in astrophysical environments is strictly connected with the emission of neutrinos. VHE astrophysical neutrinos ( $E \gtrsim 10$  TeV) detected in IceCube [39–45] are produced in connection with high-energy gamma-rays via the  $pp$  and  $p\gamma$  interactions, and they have comparable energies. The energy and angular distribution of the neutrino flux detected at IceCube points to the extragalactic origin of these neutrinos and gamma-rays. Photons with energies between a few TeV and a few PeV have a short mean free path (a few Mpc to about 10 kpc) compared to the extragalactic distances where the emitters are located. As such, these photons are not expected to reach the Earth. In presence of ALPs, however, this may become possible. Indeed, photons might convert into ALPs in the magnetic field of the source, travel unabsorbed until our Galaxy, and then convert back in the Galactic magnetic field. This setup would allow one to realize a sort of cosmic “light-shining-through-the-Universe” experiment, as proposed in different papers, see e.g. [16, 19].

Reference [46] pointed out the physics potential of current and upcoming gamma-ray detectors to constrain the photon-ALP mixing, through a measurement of the diffuse gamma-ray flux generated by extragalactic sources of 100 TeV-PeV photons. In this regard, the recent Ref. [47] used the diffuse gamma-ray signal measured by Tibet AS $\gamma$  and HAWC to search for ALPs, constraining  $g_{a\gamma} \lesssim 2.1 \times 10^{-11}$  GeV $^{-1}$  for  $m_a < 10^{-7}$  eV. Following this interesting result, we take advantage of the recent preliminary measurement of the diffuse gamma-ray flux by the Large High Altitude Air Shower Observatory (LHAASO) [48, 49] to present a new bound on ALPs, complementary to the one of Ref. [47].

The plan of our work is as follows. In Sect. 2 we discuss the expected photon spectra from the extragalactic sources exploiting the connection with the measured neutrino flux at IceCube. Then in Sect. 3 we revise the photon-ALP conversion mechanism, recalling the equations of motion for the photon-ALP ensemble and modelling the photon-ALP conversions in the magnetic field of the host galaxy and the back-conversions in the Milky-Way. We arrive in this way at characterizing the diffuse gamma-ray flux produced by the ALP conversions. In Sect. 4 we show how to obtain a

bound on the ALP-photon coupling, requiring that the diffuse photon flux produced by the ALP-photon oscillations in the Galactic magnetic field does not exceed the flux observed in LHAASO. In Sect. 5 we discuss the complementarity of our bound with other ones from very-high-energy photon observations. Finally, in Sect. 6 we summarize our results and we conclude. In Appendix we comment on the dependence of our bound on the host galaxy magnetic field, on the assumption on the star formation rate, and on the impact of a photon Galactic background on our results.

## 2 Gamma-ray sources and initial fluxes

The ALP flux entering our Galaxy originates from the gamma-ray production in the extragalactic sources of IceCube neutrinos. The extragalactic origin of IceCube neutrinos is well motivated by their energies of the order of 1 PeV, which require acceleration of cosmic-rays up to tens of PeV, a feature that is much more naturally realized in extragalactic rather than Galactic sources. Since the sources are outside of the Galaxy, they can naturally be taken as isotropically distributed. Therefore, even though the regions probed by IceCube and LHAASO are different, we can naturally extend our inferred source properties from the IceCube data to the region probed by LHAASO.

We are assuming photohadronic  $p\gamma$  (or hadronic  $pp$ ) neutrino production in a compact region inside a host galaxy. This neutrino production is accompanied by a corresponding gamma-ray production which escapes the compact region. There are two crucial assumptions here: first of all, we are assuming the compact region to be transparent for gamma-rays with energy of the order of 100 TeV. This is a tricky assumption, especially in view of the fact that the sources of IceCube neutrinos in the 10–100 TeV are likely to be gamma-ray opaque [50–52] because of the tension between the IceCube data and the diffuse gamma-ray background Fermi-LAT measurements. In fact, using a broken power-law spectrum close to our parameterization in Eq. (2) with a break energy  $E_b$ , Refs. [51, 52] show that with  $E_b \lesssim 60$  TeV explaining the IceCube data would imply a cascaded gamma-ray flux that would exceed the Fermi-LAT measurements of the extragalactic gamma-ray background. Furthermore, as noted in Ref. [50], it is quite natural for  $p\gamma$  sources of neutrinos between 25 TeV and 3 PeV to be opaque to gamma-rays between 1 GeV and 100 GeV, since the target photons for  $p\gamma$  interactions also act as a target for photon attenuation. However, this does not mean that gamma-rays above 100 TeV should be absorbed. In this higher energy range, which is of interest here, the neutrino production can be explained by gamma-ray transparent sources without exceeding the measured extragalactic gamma-ray background. Thus, current data do not suggest sources opaque to gamma-rays with these

energies, and we consider it likely that gamma-rays above 100 TeV manage to escape the compact region into the host galaxy.

Our second assumption is indeed that the neutrino sources are embedded in a galactic environment. This assumption is likely verified in most candidates proposed for explaining the IceCube data, including star-forming and starburst galaxies [53–62], active galactic nuclei [63–69], and gamma-ray bursts [70–74].

The gamma-rays associated with the IceCube neutrinos are produced by the hadronic component of cosmic-rays in the host galaxy. Under the assumptions above, they are a *guaranteed* component of the extragalactic diffuse gamma-ray flux. On the other hand, on top of it one cannot a priori exclude a contamination of gamma-rays produced leptonically. We neglect this possibility, as it would only increase the gamma-ray signal expected at Earth, and therefore would strengthen the bounds we obtain.

Concerning the neutrino flux, we follow the model in Ref. [46]. In order to exploit the neutrino-gamma connection, we consider at first photohadronic sources. In each source the neutrino spectrum is given by [46]

$$Q_\nu(E) = \frac{dN_\nu}{dEdt} \propto \left[ 1 + \left( \frac{E}{E_b} \right)^{2\alpha} \right]^{-1/2} \quad (2)$$

We consider three models from three different IceCube data analyses: the 9.5-year through-going (TG) muon neutrinos data sample [75], the 6-year cascades data sample [76], and the 7.5-year high-energy starting events (HESE) one [77]. The three models mainly differ for the spectral index  $\alpha$ , namely

$$\alpha = \begin{cases} 2.37 \text{ TG } \nu_\mu, \\ 2.48 \text{ cascades,} \\ 2.92 \text{ HESE.} \end{cases} \quad (3)$$

For all the models, the break energy is taken as  $E_b = 60$  TeV to avoid exceeding Fermi-LAT data [51, 52]. We want to point out that the different choice of  $E_b$  respect to Refs. [46, 47], where  $E_b = 25$  TeV, has no impact on the final result of this work because it does not strongly affect the detected flux at the energies of interest, close to 300 TeV. Indeed, the normalization of the neutrino spectrum in Eq. (2) is fixed from the measurement of the diffuse neutrino flux  $d\phi_\nu/dE$  at 100 TeV by inverting the following equation [47]:

$$\frac{d\phi_\nu}{dE} = \int_0^\infty \left[ (1+z)Q_\nu(E(1+z)) \right] n_s(z) \left| c \frac{dt}{dz} \right| dz \quad (4)$$

where the first term in large brackets is the emission neutrino spectrum  $Q_\nu$  for neutrinos emitted at redshift  $z$  with the prefactor of  $(1+z)$  accounting for the compression of the energy

**Table 1** Model parameters for the the source density  $n_s$ , Eq. (5), values taken from [79]. The last column reports the neutrino data we adopt to compute the source neutrino spectrum  $Q_\nu$  in the three cases

Analytic fits	$n_s(0)$	$\alpha$	$\beta$	$\gamma$	$z_1$	$z_2$	$Q_\nu$
Upper	0.0213	3.6	-0.1	-2.5	1	4	HESE
Fiducial	0.0178	3.4	-0.3	-3.5	1	4	Cascades
Lower	0.0142	3.2	-0.5	-4.5	1	4	TG $\nu_\mu$

scale, and the second term  $n_s(z)$  is the comoving source density that we assume proportional to the star formation rate (SFR), that we describe it by the functional fit of Ref. [78] so that

$$n_s(z) = n_s(0) \left[ (1+z)^{\alpha\eta} + \left( \frac{1+z}{B} \right)^{\beta\eta} + \left( \frac{1+z}{D} \right)^{\gamma\eta} \right]^{1/\eta} \quad (5)$$

where  $n_s(0)$  is the normalization (in units of  $10^{-6} \text{ Mpc}^{-3}$ ),  $B$  and  $D$  encode the redshift breaks, the transitions are smoothed by the choice  $\eta \simeq -10$ , and  $\alpha$ ,  $\beta$ , and  $\gamma$  are the logarithmic slopes of the low, intermediate, and high redshift regimes, respectively. The constants  $B$  and  $D$  are defined as

$$\begin{aligned} B &= (1+z_1)^{1-\alpha/\beta}, \\ D &= (1+z_1)^{(\beta-\alpha)/\gamma} (1+z_2)^{1-\beta/\gamma}, \end{aligned} \quad (6)$$

where  $z_1$  and  $z_2$  are the redshift breaks. All the parameters of the model are collected in Table 1 based on [79]. In Table 1 we have also reported the source neutrino spectrum that we consider for each SFR, defining Upper, Fiducial, and Lower benchmark initial neutrino fluxes.

In Fig. 1 we show the source density of Eq. (5) as a function of the redshift  $z$  for the three different set of parameters of Table 1: upper (black continuous curve), Fiducial (red dashed curve) and Lower (blue dotted curve). It is possible to observe how the maximum contribution comes from  $1 \lesssim z \lesssim 4$ , for all the cases.

Having ascertained the number of neutrinos emitted from each source, we obtain the corresponding gamma-ray spectrum by the multi-messenger relation for  $p\gamma$  interactions [80]:

$$Q_\gamma(E_\gamma) = \frac{2}{3} Q_\nu \left( \frac{E_\gamma}{2} \right) \quad (7)$$

While this relation specifically applies to neutrinos produced by photohadronic interactions, it is still valid as order of magnitude for  $pp$  sources. In Fig. 2 we show  $Q_\gamma$  as a function of the energy  $E$ , obtained considering our fiducial SFR (see Sec. III C) and the three data-sets, HESE (black dotted line), cascades (blue continuous line), and TG  $\nu_\mu$  (red dashed line).

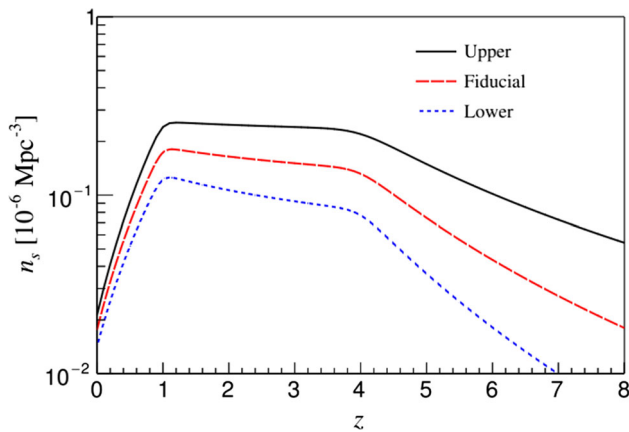


**Fig. 1** Source density  $n_s$  in function of the redshift  $z$ . We show  $n_s$  for the three sets of parameters in Table 1: upper (black continuous curve), Fiducial (red dashed curve) and lower (blue dotted curve)

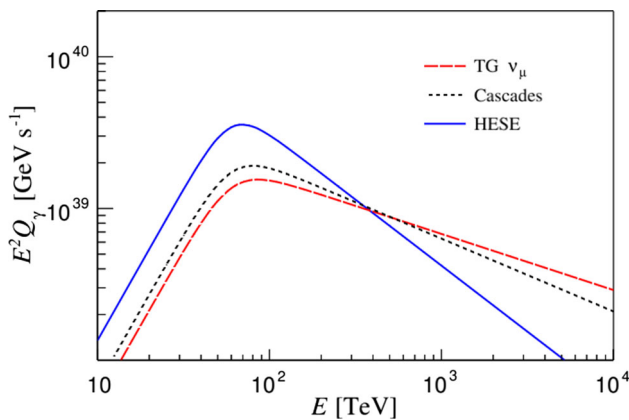


**Fig. 2** Photon spectrum  $Q_\gamma$  from a single source as a function of the energy, according to three different neutrino data-sets: TG muon neutrinos (red dashed line), cascades (black dotted line) and HESE (blue continuous line)

### 3 Photon-ALP conversions

#### 3.1 Equations of motion

The initial gamma-ray flux, in presence of ALPs, is strongly modified compared to the standard case. The Lagrangian describing the interaction between ALPs and photons is shown in Eq. (1) and it allows for ALP-photon conversions in the magnetic field of the host galaxy and the back-conversions in the large-scale Galactic magnetic field.

Assuming a monochromatic photon/ALP beam of energy  $E$  propagating along the  $x_3$  direction in a cold ionized and magnetized medium, for very relativistic ALPs and photons, the evolution can be described in terms of the Liouville equation [6, 81]

$$i \frac{d}{dx_3} \rho = [\mathcal{H}_0, \rho] - \frac{i}{2} \{\mathcal{H}_{\text{abs}}, \rho\}, \tag{8}$$

for the polarization density matrix

$$\rho(x_3) = \begin{pmatrix} A_1(x_3) \\ A_2(x_3) \\ a(x_3) \end{pmatrix} \otimes (A_1(x_3) \ A_2(x_3) \ a(x_3))^* \tag{9}$$

where  $A_1(x_3)$  and  $A_2(x_3)$  are the photon linear polarization amplitudes along the  $x_1$  and  $x_2$  axis, respectively, and  $a(x_3)$  denotes the ALP amplitude. In Eq. (8) the first commutator at right-hand-side contains the ALP-photon mixing Hamiltonian  $\mathcal{H}_0$  and the second anticommulator contains the photon absorption Hamiltonian  $\mathcal{H}_{\text{abs}}$ .

The mixing Hamiltonian  $\mathcal{H}_0$  simplifies if we restrict our attention to the case in which  $\mathbf{B}$  is homogeneous. We denote by  $\mathbf{B}_T$  the transverse magnetic field, namely its component in the plane normal to the beam direction and we choose the  $y$ -axis along  $\mathbf{B}_T$  so that  $B_x$  vanishes. The linear photon polarization state parallel to the transverse field direction  $\mathbf{B}_T$  is then denoted by  $A_{\parallel}$  and the orthogonal one by  $A_{\perp}$ . Correspondingly, the mixing matrix can be written as [82, 83]

$$\mathcal{H}_0 = \begin{pmatrix} \Delta_{\perp} & 0 & 0 \\ 0 & \Delta_{\parallel} & \Delta_{a\gamma} \\ 0 & \Delta_{a\gamma} & \Delta_a \end{pmatrix}, \tag{10}$$

whose elements are [6]:  $\Delta_{\perp} \equiv \Delta_{\text{pl}} + \Delta_{\perp}^{\text{CM}} + \Delta_{\text{CMB}}$ ,  $\Delta_{\parallel} \equiv \Delta_{\text{pl}} + \Delta_{\parallel}^{\text{CM}} + \Delta_{\text{CMB}}$ ,  $\Delta_{a\gamma} \equiv g_{a\gamma} B_T/2$  and  $\Delta_a \equiv -m_a^2/2E$ , where  $m_a$  is the ALP mass. The term  $\Delta_{\text{pl}} \equiv -\omega_{\text{pl}}^2/2E$  takes into account plasma effects, in terms of the plasma frequency  $\omega_{\text{pl}}$  expressed as a function of the electron density in the medium  $n_e$  as  $\omega_{\text{pl}} \simeq 3.69 \times 10^{-11} \sqrt{n_e/\text{cm}^{-3}} \text{ eV}$ . The terms  $\Delta_{\parallel, \perp}^{\text{CM}}$  represent the Cotton–Mouton effect, accounting for the birefringence of fluids in the presence of a transverse magnetic field. A vacuum Cotton–Mouton effect is expected from QED one-loop corrections to the photon polarization in the presence of an external magnetic field  $\Delta_{\text{QED}} \propto |\Delta_{\perp}^{\text{CM}} - \Delta_{\parallel}^{\text{CM}}| \propto B_T^2$ , precisely  $\Delta_{\parallel} = \frac{7}{2} \Delta_{\text{QED}}$  and  $\Delta_{\perp} = 2 \Delta_{\text{QED}}$  [6]. Finally, the term  $\Delta_{\text{CMB}} \propto \rho_{\text{CMB}}$  represents the background photon contribution to the photon polarization [84]. An off-diagonal  $\Delta_R$  would induce the Faraday rotation, which is however totally irrelevant at VHE, and so it has been dropped. For relevant parameters at redshift  $z = 0$  we use

$$\begin{aligned} \Delta_{a\gamma} &\simeq 1.5 \times 10^{-2} \left( \frac{g_{a\gamma}}{10^{-11} \text{ GeV}^{-1}} \right) \left( \frac{B_T}{10^{-6} \text{ G}} \right) \text{ kpc}^{-1}, \\ \Delta_a &\simeq -0.8 \times 10^{-4} \left( \frac{m_a}{10^{-8} \text{ eV}} \right)^2 \left( \frac{E}{10^2 \text{ TeV}} \right)^{-1} \text{ kpc}^{-1}, \\ \Delta_{\text{pl}} &\simeq -1.1 \times 10^{-12} \left( \frac{E}{10^2 \text{ TeV}} \right)^{-1} \left( \frac{n_e}{10^{-3} \text{ cm}^{-3}} \right) \text{ kpc}^{-1}, \\ \Delta_{\text{QED}} &\simeq 6.1 \times 10^{-4} \left( \frac{E}{10^2 \text{ TeV}} \right) \left( \frac{B_T}{10^{-6} \text{ G}} \right)^2 \text{ kpc}^{-1}, \\ \Delta_{\text{CMB}} &\simeq 8.0 \times 10^{-3} \left( \frac{E}{10^2 \text{ TeV}} \right) \text{ kpc}^{-1}, \end{aligned} \tag{11}$$



where the expression for  $\Delta_{\text{CMB}}$  is a valid approximation for  $E < 100$  TeV. We will provide later the complete expression used in our work.

VHE photons undergo pair production absorptions by background low energy photons  $\gamma_{\text{VHE}} + \gamma_{\text{EBL}} \rightarrow e^+ + e^-$ . We emphasize that we are assuming the compact source inside the host galaxy to be gamma-ray transparent, and are only accounting for absorption in the larger host environment and in the Milky-Way. The absorptive part of the Hamiltonian in Eq. (8) can be written in the form

$$\mathcal{H}_{\text{abs}} = \begin{pmatrix} \Gamma & 0 & 0 \\ 0 & \Gamma & 0 \\ 0 & 0 & 0 \end{pmatrix}, \tag{12}$$

where  $\Gamma$  is the VHE photon absorption rate, which as a function of the incident photon energy  $E$  is given by [85] (see also [18])

$$\Gamma(E) = \int_{m_e^2/E}^{\infty} d\epsilon \frac{dn_{\gamma}^{\text{bkg}}}{d\epsilon} \int_{-1}^{1 - \frac{2m_e^2}{E\epsilon}} d\xi \frac{1 - \xi}{2} \sigma_{\gamma\gamma}(\beta), \tag{13}$$

where the limits of integration in both integrals are determined by the kinematical threshold of the process and

$$\sigma_{\gamma\gamma}(\beta) = \sigma_0(1 - \beta^2) \left[ 2\beta(\beta^2 - 2) + (3 - \beta^4) \log \frac{1 + \beta}{1 - \beta} \right],$$

with  $\sigma_0 = 1.25 \times 10^{-25} \text{ cm}^2$ , is the cross section for the pair production process [86] as a function of the electron velocity in the center of mass frame  $\beta = [1 - 2m_e^2/E\epsilon(1 - \xi)]^{1/2}$ . Here  $\epsilon$  is the background photon energy, and  $\xi$  is the cosine of the angle between the incident and the background photon. The photon background spectrum  $dn_{\gamma}^{\text{bkg}}/d\epsilon$  takes into account the  $\gamma$  absorption caused by cosmic microwave background (CMB), and in the Milky Way we also account for the presence of starlight (SL) and infrared (IR) backgrounds. The SL+IR background is extracted from the GALPROP code [87].

In the upper panel of Fig. 3 we show the VHE photon absorption rate, obtained from Eq. (13), as a function of the photon energy  $E$ , for the host galaxy (red dashed lines) and the Milky Way near the Sun (black continuous line). The changing of the slope of the Milky Way  $\Gamma$  reflects the three components of  $dn_{\gamma}^{\text{bkg}}/d\epsilon$  (CMB, SL and IR). Due to these components, the absorption rate is monotonically increasing for almost all the energy range considered. Only at very-high-energies ( $E_{\gamma} > 3 \times 10^3$  TeV),  $\Gamma$  decreases as expected, reflecting the decreasing behaviour of  $\sigma_{\gamma\gamma}$  for  $\beta \rightarrow 1$ . The absorption term  $\Gamma$  dominates the mixing term  $\Delta_{a\gamma}$  for  $E > 10^3$  TeV for  $B = 5 \mu\text{G}$  and  $g_{a\gamma} < 2.0 \times 10^{-11} \text{ GeV}^{-1}$ .

Once obtained  $\Gamma$ , we can calculate the  $\Delta_{\text{CMB}}$  parameter as discussed in Ref. [84]:

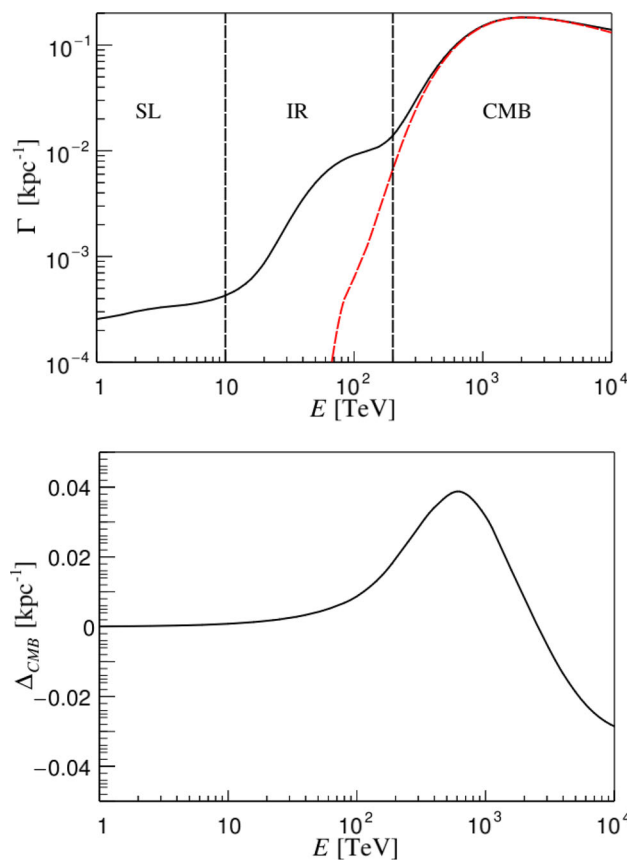


**Fig. 3** Upper panel: VHE photon absorption rate as a function of the photon energy  $E$  for the host galaxy (red dashed curves) and the Milky Way near the Sun, using the  $dn_{\gamma}^{\text{bkg}}/d\epsilon$  in Ref. [84] (black continuous curves). Lower panel:  $\Delta_{\text{CMB}}$  factor as a function of the photon energy  $E$  obtained with Eq. (14)

$$\Delta_{\text{CMB}} = \frac{E}{\pi} \times \text{p.v.} \int_0^{\infty} dE' \frac{\Gamma(E')}{E'^2 - E^2}, \tag{14}$$

where p.v. indicates the Cauchy principal value integral. This expression is valid in all the range of energy of our interest, i.e.  $1 \text{ TeV} < E < 10^4 \text{ TeV}$ , and we use it in the conversion probability evaluation. In the lower panel of Fig. 3 we show the  $\Delta_{\text{CMB}}$  parameter as a function of the photon energy  $E$ . One realizes that at  $E > 10^2$  TeV there are strong deviations with respect to the naive linear dependence of Eq. (11), reflecting the behaviour of the absorption factor  $\Gamma$ .

### 3.2 Photon-ALP conversions in the host galaxy

In principle the cosmic accelerators producing neutrinos and photons may host strong magnetic fields  $B \sim \mathcal{O}(1 - 10) \mu\text{G}$  (see, e.g., [29, 88, 89]). However, due to the severe uncertainties in the characterization of these fields, we conservatively neglect this possibility. Besides being conservative, this is also pretty realistic: within the compact region, one needs rather strong magnetic fields to achieve an efficient conver-

sion. However, large magnetic fields actually inhibits, rather than enhance, the photon-ALP conversion in the compact region, because of the large photon refraction in the magnetic field due to  $\Delta_{\text{QED}}$ . Therefore, the conversion in the compact region is likely subdominant compared to the conversion in the host galaxy. Therefore, we consider at first the conversions of the gamma-ray flux in the host galaxies where the sources are embedded. Concerning the strength of the magnetic fields, one expects values and morphology similar to our Milky Way (see Refs. [90–92] for recent studies). Furthermore, a combination of regular and turbulent components might be present. However, due to the presence of large uncertainties in the description of these source fields, we assume two simplified models. Namely (a) a box of constant magnetic field, mimicking in this way a regular field, (b) a cell model where in each domain the magnetic field can change strength and direction, like in Ref. [46]. This latter model would represent the pure turbulent case.

### 3.2.1 Box model

We start considering the propagation of photons in a single magnetic domain with a uniform  $\mathbf{B}$ -field with  $B_x = 0$ , the component  $A_\perp$  decouples away, and the propagation equations reduce to a two-dimensional problem. Its solution follows from the diagonalization of the Hamiltonian through a similarity transformation performed with an orthogonal matrix, parametrized by the (complex) rotation angle  $\Theta$  which takes the value [6,81]

$$\Theta = \frac{1}{2} \arctan \left( \frac{2\Delta_{a\gamma}}{\Delta_\parallel - \Delta_a - \frac{i}{2}\Gamma} \right). \tag{15}$$

When  $\Delta_{a\gamma} \gg \Delta_\parallel - \Delta_a$  the photon-ALP mixing is close to maximal,  $\Theta \rightarrow \pi/4$  (if the absorption is small as well). On the other hand, from Fig. 3 one sees that for  $E < 10^3$  TeV  $\Delta_{\text{CMB}}$  grows with the photon energy. Therefore at sufficiently high energies  $\Delta_{a\gamma} \ll \Delta_\parallel - \Delta_a$  and the photon-ALP mixing is suppressed.

One can introduce a generalized (including absorption) photon-ALP oscillations frequency

$$\Delta_{\text{osc}} \equiv \left[ (\Delta_\parallel - \Delta_a - \frac{i}{2}\Gamma)^2 + 4\Delta_{a\gamma}^2 \right]^{1/2}. \tag{16}$$

As noticed before, for  $E \lesssim 10^3$  TeV the absorption effects are subleading. In this situation the probability for a photon emitted in the state  $A_\parallel$  to oscillate into an ALP after traveling a distance  $L$  is given by [6]

$$\begin{aligned} P_{\gamma \rightarrow a}^s &= \sin^2 2\Theta \sin^2 \left( \frac{\Delta_{\text{osc}} L}{2} \right) \\ &= (\Delta_{a\gamma} L)^2 \frac{\sin^2(\Delta_{\text{osc}} L/2)}{(\Delta_{\text{osc}} L/2)^2}, \end{aligned} \tag{17}$$

where in the oscillation wave number and mixing angle we set  $\Gamma = 0$ . It is also useful to define a critical energy, above which  $P_{a\gamma} \simeq 0$ . Similarly to Ref. [93], the terms in  $\Delta_{\text{osc}}$  can be rearranged such that a critical energy is defined as

$$\begin{aligned} E_c &= \frac{2\Delta_{a\gamma} E}{\Delta_\parallel + \Delta_{\text{CMB}}} \\ &= \frac{2.14 \times 10^3 \text{ TeV}}{\left(\frac{B}{\mu\text{G}}\right)^2 + 5.71} \left( \frac{g_{a\gamma}}{10^{-11} \text{ GeV}^{-1}} \right) \left( \frac{B}{\mu\text{G}} \right). \end{aligned} \tag{18}$$

Therefore, one expects that the conversion probability would be already strongly suppressed before absorption effects become relevant.

For definiteness, we assume values of the magnetic field for the host galaxies in the ballpark of what suggested by observational constraints [90–92]. In particular we take  $B_T = (5 \pm 3) \mu\text{G}$ , constant on a box with  $L = (5 \pm 3)$  kpc. In Fig. 4 we show the value of the conversion probability  $P_{\gamma \rightarrow a}^s$  as a function of the host-galaxy size for  $E = 10$  TeV,  $g_{a\gamma} = 3 \times 10^{-11} \text{ GeV}^{-1}$  and  $B_T = 8 \mu\text{G}$  (red continuous line), and  $B_T = 5 \mu\text{G}$  (black continuous line). This result must be averaged over the photon polarization, assuming unpolarized light. Because of the oscillating behavior with distance, with wavelength comparable to the propagation length, we choose to average over the path traversed by the photon as well:

$$\langle P_{\gamma \rightarrow a}^s \rangle = \frac{1}{2} \times \frac{\int_{L_{\text{min}}}^{L_{\text{max}}} dL P_{\gamma \rightarrow a}^s}{\Delta L}, \tag{19}$$

where  $L_{\text{min}} = 2$  kpc,  $L_{\text{max}} = 8$  kpc,  $\Delta L = 6$  kpc, and the factor  $1/2$  takes into account the average over the two photon polarization states. The averaged probabilities are also shown in Fig. 4 in dashed curves. It results that the case of  $B_T = 5 \mu\text{G}$  presents a larger  $\langle P_{\gamma \rightarrow a}^s \rangle$  than the case with  $B_T = 8 \mu\text{G}$  because of the choice of magnetic model, which gives an oscillation length comparable with the extension of the magnetic field.

### 3.2.2 Cell model

As a second case, following Ref. [46] we consider a different model for the source magnetic field to represent the turbulent case. The field is assumed to be divided into cells, whose length is fixed to  $l = 1$  kpc and where  $\mathbf{B}$  has fixed strength and direction. In each cell, the  $\mathbf{B}_T$  components are variable and follow a Gaussian distribution with zero mean and variance  $2B_T^2/3$ , such that  $\langle |\mathbf{B}_T| \rangle = B_T$ . We obtain the mean probability in each cell  $\langle P_{\gamma \rightarrow a} \rangle$  by averaging over the Gaussian distribution of  $B_T$ . Then, to obtain the conversion probability for  $n$  domains of length  $l$ , we follow the treatment in Ref. [81] to which we address the reader for further

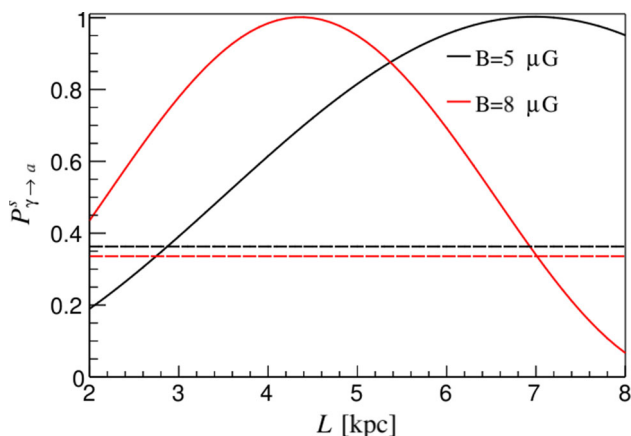


**Fig. 4** Photon-ALP conversion probability in the host-galaxy as a function of the source size  $L$  for the case of a regular field, for  $E = 10$  TeV,  $g_{a\gamma} = 3 \times 10^{-11}$  GeV $^{-1}$  and  $z = 0$ . We consider two values of the magnetic field:  $B_T = 8 \times 10^{-6}$  G (red curves) and  $B_T = 5 \times 10^{-6}$  G (black curves). The continuous curves represent the probability  $P_{\gamma \rightarrow a}^s(L)$ , while the dashed ones represent the average  $\langle P_{\gamma \rightarrow a}^s \rangle$

details. Finally, we obtain the total conversion probability in the source  $\langle P_{\gamma \rightarrow a}^s \rangle$  averaging over the host-galaxy size.

In Fig. 5 we show the average conversion probability  $\langle P_{\gamma \rightarrow a}^s \rangle$  for the single box magnetic field (continuous curves) and for the cell model (dashed curves). We take  $g_{a\gamma} = 3 \times 10^{-11}$  GeV $^{-1}$  and  $z = 0$ . Concerning the magnetic field, we take  $B_T = 5 \mu\text{G}$  (black curves) and  $B_T = 8 \mu\text{G}$  (red curves). The general trend of the probabilities is quite similar for the two models. However, the absolute value in the energy-independent region ( $E < 10^2$  TeV) is smaller in the cell model case due to the less efficient conversions because of the loss of coherence after each cell. Conversely, at higher energies one finds an opposite trend because of the reduced suppression proportional to the average magnetic field magnitude (see Eq. (18)). On the other hand, when  $E$  approaches  $E_c \sim 10^3$  TeV [see Eq. (18)] the conversion probability drops till it becomes negligible in both cases.

### 3.3 Impact of the redshift

Till now all the considerations we have done neglect the effect of redshift on the photon-ALP conversions. However, as evident from Fig. 1 one expects the largest contributions from photon sources at  $1 \lesssim z \lesssim 4$ . Therefore, redshift effects should be taken into account as we describe in this Section.

The redshift effects leave unaltered the equations of motion [Eq. (8)], after an appropriate rescaling of the different parameters, as we now explain. Since the number density of the electrons traces that of matter, and the average number density of electrons goes as the third power of the size of the Universe, we obtain the relationship

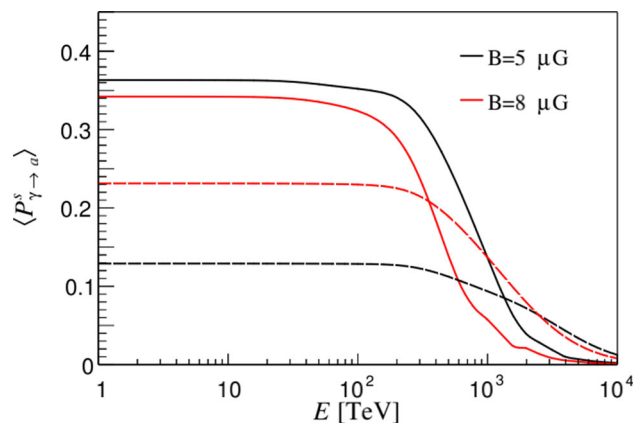


**Fig. 5** Average  $\langle P_{\gamma \rightarrow a}^s \rangle$  conversion probabilities in the host galaxy at  $z = 0$  as a function of the energy  $E$ . We take  $g_{a\gamma} = 3 \times 10^{-11}$  GeV $^{-1}$  and consider  $B_T = 8 \times 10^{-6}$  G (red curves) and  $B_T = 5 \times 10^{-6}$  G (black curves). The continuous curves are for a single box regular  $B$ -field, while the dashed curves refer to the turbulent cell model

$$n_e(z) = n_{e,0}(1+z)^3. \tag{20}$$

This is the redshift effect entering the plasma frequency  $\omega_{\text{pl}}$ . Concerning the  $B$ -field in the host galaxy, in principle one should take into account a possible evolution as a function of the redshift [94]. However, there is no clear picture in the trend of this effect, see e.g. Ref. [95]. Therefore we prefer to assume no redshift dependence in the host magnetic field. Moreover, we have not assumed a scaling of the magnetic cells size in the source [96], while the energy of the beam scales as

$$E(z) = E_0(1+z), \tag{21}$$

where with subscript 0 we indicate the today values of the different quantities. Considering these redshift relations, we find that the quantities in Eq. (11) evolve as

$$\begin{aligned} \Delta_{a\gamma} &= \Delta_{a\gamma}^0, \\ \Delta_a &= \frac{\Delta_a^0}{(1+z)}, \\ \Delta_{\text{pl}} &= \Delta_{\text{pl}}^0(1+z)^2, \\ \Delta_{\text{QED}} &= \Delta_{\text{QED}}^0(1+z), \end{aligned}$$

where the superscript 0 indicates the today value. Concerning the absorption factor  $\Gamma$  in Eq. (13) one has to properly redshift the background photon energy  $\epsilon$ , the VHE photon  $E$  and the photon background density  $\text{bkg}_\gamma$ . In particular, as discussed above for  $E \gtrsim 10^3$  TeV the main contribution to the cosmic opacity is associated with CMB photon background. In this situation the redshifted expression of  $\Gamma$  is analytical. Indeed, the CMB background spectra scales as

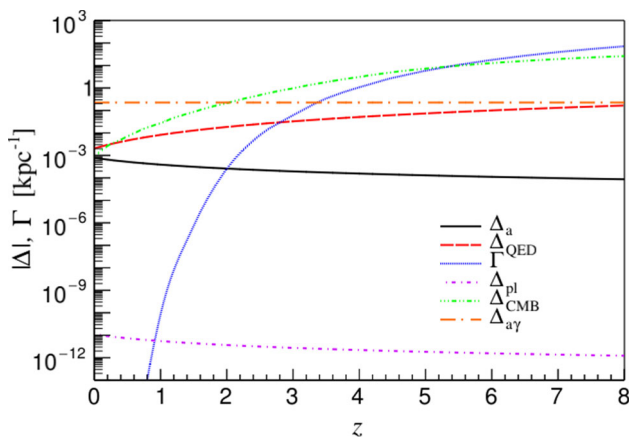


**Fig. 6** Redshift evolution of the factors  $\Delta_a$  (black continuous curve),  $\Delta_{\text{QED}}$  (red dashed curve),  $\Gamma$  (blue dotted curve),  $\Delta_{\text{pl}}$  (magenta dot-dashed curve),  $\Delta_{\text{CMB}}$  (green dot-dashed curve) and  $\Delta_{a\gamma}$  (orange long dot-dashed curve) evaluated at  $E = 10 \text{ TeV}$ ,  $B = 5 \mu\text{G}$ ,  $m_a \ll 10^{-7} \text{ eV}$  and  $g_{a\gamma} = 3 \times 10^{-11} \text{ GeV}^{-1}$

$$\frac{dn_{\gamma}^{\text{CMB}}}{d\epsilon} = \frac{\epsilon^2}{\pi^2} \frac{1}{e^{\epsilon/T_{\text{CMB}}(1+z)} - 1} \tag{22}$$

Then, with the change of variable  $\epsilon' = \epsilon/(1+z)$  in Eq. (13) it can be shown that  $\Gamma$  scales as

$$\begin{aligned} \Gamma(E, z) &= (1+z)^3 \Gamma(E(1+z), z=0) \\ &= (1+z)^3 \Gamma(E_0(1+z)^2, z=0), \end{aligned} \tag{23}$$

where the factor  $(1+z)^3$  accounts for the increasing for the background photon number density of the redshift and the scaling  $E(1+z)$  in the energy is due to the increasing in energy of the background photon. The maximum of absorption thus shifts to lower energies when  $z$  increases. From the scaling of  $\Gamma(E, z)$  and Eq. (14) one can obtain that the redshift of  $\Delta_{\text{CMB}}(E, z)$  follows the same law.

In Fig. 6, we show the evolution in  $z$  of the relevant quantities, in Eq. (11), for  $E = 10 \text{ TeV}$ ,  $B = 5 \mu\text{G}$ ,  $m_a \ll 10^{-7} \text{ eV}$  and  $g_{a\gamma} = 3 \times 10^{-11} \text{ GeV}^{-1}$ . It is clear that the suppression of the conversion probability  $\langle P_{\gamma \rightarrow a} \rangle$  starts at  $z \sim 2-3$ , when  $\Gamma \gtrsim \Delta_{a\gamma}, \Delta_{\text{QED}}$ .

In Fig. 7 we show the averaged conversion probability  $\langle P_{\gamma \rightarrow a}^s \rangle$  in function of the redshift  $z$  of the host galaxy. We consider the single box magnetic field (continuous curves) and for the cell model (dashed curves). We take  $g_{a\gamma} = 3 \times 10^{-11} \text{ GeV}^{-1}$  and  $E = 10 \text{ TeV}$ . As in Fig. 5, we take  $B_T = 5 \mu\text{G}$  (black curves) and  $B_T = 8 \mu\text{G}$  (red curves). The general trend is a reduction of the conversion probability at increasing  $z$  due to the increasing of the  $\Gamma$  and  $\Delta_{\text{CMB}}$  factors over  $z$ , as it is possible to see in Fig. 6. For  $z > 2$ ,  $\langle P_{\gamma \rightarrow a} \rangle$  is suppressed as a consequence of  $\Delta_{\text{CMB}} > \Delta_{a\gamma}$ . Moreover  $\langle P_{\gamma \rightarrow a}^s \rangle$  in the single box model drops to zero before that

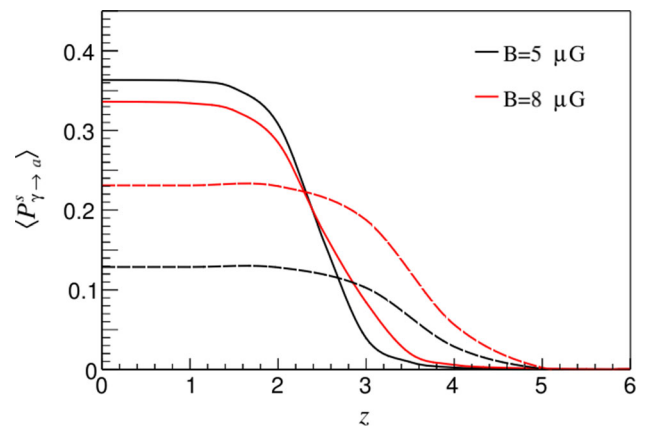


**Fig. 7** Average  $\langle P_{\gamma \rightarrow a}^s \rangle$  conversion probabilities in the host galaxy at  $E = 10 \text{ TeV}$  as a function of the redshift  $z$  of the source. We take  $g_{a\gamma} = 3 \times 10^{-11} \text{ GeV}^{-1}$  and consider  $B_T = 8 \times 10^{-6} \text{ G}$  (red curves) and  $B_T = 5 \times 10^{-6} \text{ G}$  (black curves). The continuous curve are for a single box regular  $B$ -field, while the dashed curves refer to the cell model

in the cell model, similarly to what happen for the energy evolution in Fig. 5.

### 3.4 Diffuse ALP flux

As next step we determine the diffuse ALP flux produced by VHE gamma-ray conversions in the different host galaxies. In analogy with the diffuse neutrino flux of Eq. (4) we write [47]

$$\begin{aligned} \frac{d\phi_a}{dE} &= \int_0^\infty \left[ (1+z) Q_\gamma(E(1+z)) \right] \\ &\quad \times \left\langle P_{a\gamma}^s(E(1+z)) \right\rangle n_s(z) \left| c \frac{dt}{dz} \right| dz, \end{aligned} \tag{24}$$

where we added the conversion probability in the host galaxy  $\langle P_{a\gamma}^s \rangle$  computed at the emission energy  $E(1+z)$ .

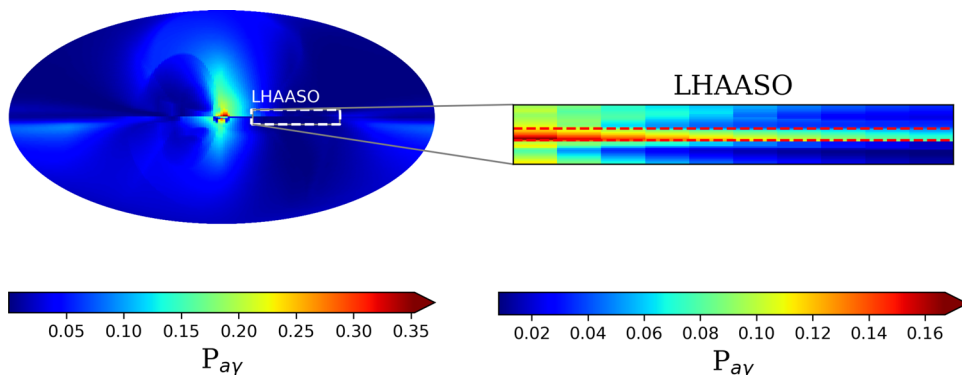
### 3.5 ALP-photons back-conversions in the Milky-Way

After ALPs and photons leave the host galaxy in which the source is placed, they propagate in the extragalactic space. At the energy we are considering ( $E > 10 \text{ TeV}$ ) the photons are completely absorbed due to the high intergalactic medium opacity. Instead, ALPs propagate unimpeded. Due to the uncertainty in the extragalactic magnetic field, we assume it sufficiently small in order to avoid ALP-photon conversions in the extragalactic space (see, however, Ref. [25] for possible effects). When ALPs reach the edge of the Milky-Way, back-conversions into gamma-rays might occur in the Galactic  $B$ -field. Then, the gamma-ray flux at Earth is given by

$$\frac{d\phi_{\gamma, \oplus}}{dE} = P_{a\gamma}^{\text{MW}} \frac{d\phi_a}{dE}, \tag{25}$$



**Fig. 8** Skymap of the conversion probability in the Galaxy for  $g_{a\gamma} = 3 \times 10^{-11} \text{ GeV}^{-1}$ ,  $m_a \ll 10^{-7} \text{ eV}$  and  $E = 10 \text{ TeV}$ . The regions probed by LHAASO is highlighted by the white dashed line and the region approximately defined by  $b \in [-1^\circ, 1^\circ]$  is masked to avoid contamination by known sources in the Galactic plane



where  $d\phi_{\gamma,\oplus}/dE$  is the photon flux reaching the Earth,  $d\phi_a/dE$  is the flux obtained from Eq. (24) and  $P_{a\gamma}^{\text{MW}}$  is the photon-ALP conversion probability in the Milky-Way.

We model the Galactic magnetic field as described by the Jansson-Farrar model [97] with the updated parameters given in Tab. C.2 of Ref. [98] (“Jansson12c” ordered fields) and an electron density in the Galaxy described by the model in Ref. [99]. The ALP propagation and mixing in the Galaxy is a purely three-dimensional problem because of the highly non-trivial structure of the magnetic field (note that we neglect the small-scale turbulent field [33]). Therefore, both the photon polarization states play a role in the oscillation phenomenon. We have closely followed the technique described in Refs. [19, 100] to solve Eq. (8) along a Galactic line of sight and obtain the back-conversion probability  $P_{a\gamma}^{\text{MW}}$  for the produced ALP. In Fig. 8 we show the skymap of the conversion probability  $P_{a\gamma}^{\text{MW}}$  for  $g_{a\gamma} = 3 \times 10^{-11} \text{ GeV}^{-1}$ ,  $m_a \ll 10^{-7} \text{ eV}$  and  $E = 10 \text{ TeV}$ , as well as the region probed by LHAASO, corresponding to galactic longitude  $25^\circ < l < 100^\circ$  and latitude  $1^\circ < |b| < 5^\circ$ . The coordinates in the plot correspond to a Mollweide projection with positive longitudes on the right of the plot. It results that the averaged  $P_{a\gamma}^{\text{MW}} \sim 10^{-2}$  in the region of interest probed by LHAASO. Note that a strip of  $1^\circ$  around the Galactic plane is not considered since the LHAASO measurement masked this region to avoid contamination by known sources, which are abundant in the Galactic plane. Finally, in Fig. 9 we show the produced photon flux in the Galaxy due to ALP conversions. For definiteness, we assume the box model of the host galaxy  $B$  field with  $B_T = 5 \mu\text{G}$ , and the Fiducial case of Table 1 for the photon spectrum in source. We take  $g_{a\gamma} = 3 \times 10^{-11} \text{ GeV}^{-1}$  (blue continuous line) and  $g_{a\gamma} = 4 \times 10^{-11} \text{ GeV}^{-1}$  (green dashed line). LHAASO data points [49] are also shown. In the next Section we will show how to obtain a bound in the plane  $g_{a\gamma}$  vs  $m_a$  requiring that the produced photons flux does not exceed the experimental one.

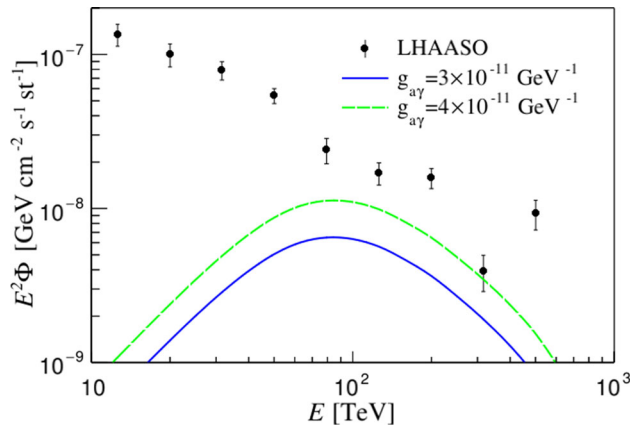


**Fig. 9** Expected photon flux from ALP conversions. We assume the box model of the host galaxy  $B$  field with  $B_T = 5 \times 10^{-6} \text{ G}$  and the Fiducial case of Table 1 for the photon spectrum in source. We show cases with  $g_{a\gamma} = 3 \times 10^{-11} \text{ GeV}^{-1}$  (blue continuous line) and  $g_{a\gamma} = 4 \times 10^{-11} \text{ GeV}^{-1}$  (green dashed line). LHAASO data points are also shown

### 4 Analysis and results

To constraints the ALP parameter space, we perform a chi-squared analysis with

$$\chi^2 = \sum_{i=1}^N \begin{cases} \left( \frac{\frac{d\phi_{\gamma,\oplus}^i}{dE} E_i^2 - \frac{d\phi_{\gamma,\text{exp}}^i}{dE} E_i^2}{\sigma(E_i)} \right)^2 & \left( \frac{d\phi_{\gamma,\text{exp}}^i}{dE} \leq \frac{d\phi_{\gamma,\oplus}^i}{dE} \right) \\ 0 & \text{(otherwise)} \end{cases} \tag{26}$$

where  $N$  is the number of LHAASO data points,  $E_i^2 d\phi_{\gamma,\text{exp}}^i/dE$  are the experimental measurements and  $\sigma(E_i)$  are the errors associated to those data.

The quantity defined in Eq. (26) follow an half- $\chi^2$  distribution. Then we can exclude the values of  $g_{a\gamma}$  for which  $\chi^2 > 2.71$  to obtain bounds at 95% confidence level (C.L.). We take as benchmark case the host galaxy magnetic field as a single box with  $B_T = 5 \mu\text{G}$ , the Fiducial case of Table 1 and no photon background in the Milky-Way. In the Appendix

**Table 2** Uncertainties on the ALP-photon coupling  $g_{a\gamma}$  constraint, varying the condition of the benchmark case. The last row indicates the total uncertainty range when all sources are combined to form a most optimistic and most pessimistic scenario

Source of uncertainties	Absolute [ $10^{-11}$ GeV $^{-1}$ ]	Relative [%]
$Q_\nu$ and $Q_\gamma$	[4.25, 5.00]	17
$B$ field	[4.90, 7.40]	51
photon bkg	[4.35, 4.85]	11
total	[3.90, 7.80]	100

we comment the dependence of our bound on the host galaxy magnetic field, on the assumption on the star formation rate and on the presence of a photon Galactic background. We summarize the impact of these factors on the final bound on  $g_{a\gamma}$  in Table 2. We realize that the largest uncertainty on the bound is due to the unknown value of the magnetic field in the host galaxy, leading up to  $\sim 50\%$  of uncertainty.

Taking into account all the uncertainty we obtain a band in our exclusion plot shown in blue in Fig. 10 at 95% C.L. The strongest constraint gives  $g_{a\gamma} < 3.9 \times 10^{-11}$  GeV $^{-1}$  for  $m_a < 10^{-7}$  eV and corresponds to  $B_T \sim 5 \mu\text{G}$  (single box model), Upper case and photon background (light blue area). Conversely the less restrictive bound gives  $g_{a\gamma} < 7.8 \times 10^{-11}$  GeV $^{-1}$  for  $m_a < 10^{-7}$  eV and corresponds to  $B_T = 2 \mu\text{G}$  (cell model), Lower case without photon background (blue area). Finally, the black dashed curve corresponding to  $g_{a\gamma} = 4.8 \times 10^{-11}$  GeV $^{-1}$  is obtained for the benchmark case described above. We notice that the bound is independent on the ALP mass for  $m_a < \mathcal{O}(10^{-7}$  eV), while it deteriorates for higher values of the mass due to the mass suppression effect of the conversion probability.

## 5 Comparison of the bounds

In this section we compare our new bound with other ones in the same range of the ALP parameter space. As custom, for comparison we take as reference the CAST bound on solar ALPs [101]. We realize that in the worst case our bound is slightly above the CAST bound (and to the stellar bound on helium-burning stars [102]), namely  $g_{a\gamma} < 6.6 \times 10^{-11}$  GeV $^{-1}$ . Conversely, in the most optimistic case we improve the CAST bound by a factor  $\sim 2$ .

In Fig. 10, we also show other complementary bounds in the same region of the ALP parameter space from gamma-ray observations from astrophysical sources. For ALPs with masses  $m_a \lesssim 10^{-9}$  eV, the strongest bound on  $g_{a\gamma}$  is derived from the absence of gamma-rays from SN 1987A, giving  $g_{a\gamma} < 5 \times 10^{-12}$  GeV $^{-1}$  for  $m_a \lesssim 10^{-10}$  eV [103]. A comparable bound on  $g_{a\gamma}$  has been recently extended in the mass range  $0.5 \lesssim m_a \lesssim 5$  neV from the nonobservation

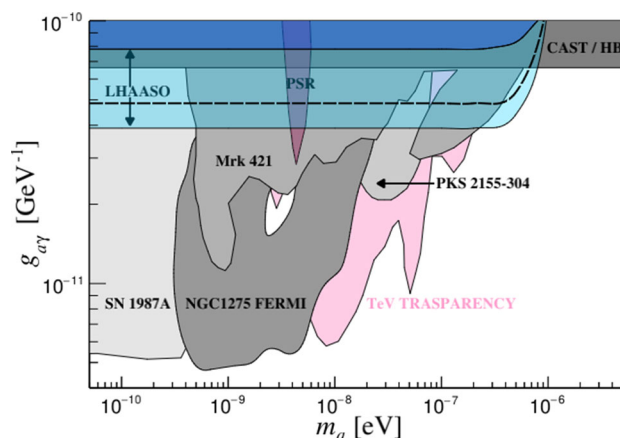


**Fig. 10** Exclusion plots in the parameter space  $g_{a\gamma}$  vs  $m_a$  from gamma-ray observations. The LHAASO bounds are in blue, where the range dark-light blue depends on the assumptions of the magnetic field in the source and on the initial gamma-ray spectrum, and the dashed line represents our benchmark case. For comparison it is shown also the CAST bound on solar ALPs [101], comparable with the stellar bound on helium-burning stars [102]. Other astrophysical bounds are in grey: namely the SN 1987A [103], the Fermi-LAT one on NGC 1275 [24], the H.E.S.S. bound on PKS 2155-304 [21], the Mrk 421 [104]. It is shown also the region hinted by the spectral modulations of pulsars (PSR) [105]. In magenta it is shown region where ALP conversions would affect the transparency of TeV photons [20]

in Fermi-LAT data of irregularities induced by photon-ALP conversions in the gamma-ray spectrum of NGC 1275, the central galaxy of the Perseus Cluster [106]. Data from the H.E.S.S. observations of the distant BL Lac object PKS 2155-304 also limit  $g_{a\gamma} < 2.1 \times 10^{-11}$  GeV $^{-1}$  for  $15 \lesssim m_a \lesssim 60$  neV [107]. Finally, other limits have been obtained by the ARGO-YBJ and Fermi-LAT observations of Mrk 421, which find an upper limit on  $g_{a\gamma}$  in the range  $[2 \times 10^{-11}, 6 \times 10^{-11}]$  GeV $^{-1}$  for  $5 \times 10^{-10} \lesssim m_a \lesssim 5 \times 10^{-7}$  eV [104].

However, these latter bounds strongly depend on severe uncertainties on the characterization of the magnetic field in the source and in the galaxy clusters. In this context, the choice of pure turbulent field in galaxy clusters has been recently criticized in Ref. [108] (see also Ref. [105]) showing that assuming a regular magnetic field the bound would be strongly relaxed, being confined above the CAST exclusion region. As we have shown, since our bound is not based on the detection of irregular modulations of the gamma-ray spectrum, it is less sensitive to the uncertainty of the magnetic fields.

We also show the region (PSR) hinted by the spectral modulation observed in gamma-rays from Galactic pulsars and supernova remnants, that can be attributed to conversions into ALPs with a mass  $m_a \sim 4 \times 10^{-9}$  eV and  $g_{a\gamma} \sim 2 \times 10^{-10}$  GeV $^{-1}$  [105]. Apparently, this region is in contrast with CAST bound and with SN 1987A. However, it has been proposed in Ref. [105] that these bounds, relying on ALPs production in astrophysical plasmas might be evaded,

assuming environmental effects suppressing the in-medium ALP-photon coupling. At this regard, our new bound being based only on conversion effects would totally or partially constrain the PSR hinted area.

Our bound is very similar to the recent one of Ref. [47] based on the diffuse gamma-ray signal measured by Tibet AS $\gamma$  and HAWC which constrain  $g_{a\gamma} \lesssim 2.1 \times 10^{-11} \text{ GeV}^{-1}$  for  $m_a < 10^{-7} \text{ eV}$ . The main differences come from the consideration of a photon background evaluated from the data of HAWC and Tibet AS $\gamma$  [109] which is not simultaneously compatible with the LHAASO data-set.

Our bound still leaves a significant region of the parameter space that can be probed by the future Cherenkov Telescope Array [23,110], especially in connection with the region where ALP conversions would affect the TeV photon transparency (magenta region) [20]. However, at this regard, we mention that in Ref. [111] recently it has been presented a limit on  $g_{a\gamma}$  from magnetic white dwarf polarization, that would be in tension with all the region hinted by the TeV photon anomalous transparency.

## 6 Conclusions

The latest data of VHE gamma-rays measured by LHAASO have been used to constrain the ALP properties. Precisely, photons produced in extragalactic sources convert into ALPs in the magnetic field of the source forming a diffuse ALP flux that propagates unhindered (by contrast with photons that are absorbed) and re-convert into photon in the Galactic magnetic field. It is possible that this non-standard contribution to the VHE diffuse flux is sizable, leaving some imprints in the photon energy spectrum measured by LHAASO. Indeed, in the presence of ALPs one expects a larger photon flux compared to the standard case. We performed an analysis based on the latest LHAASO data in the energy range 10–500 TeV to constrain the ALP-induced photon flux and then the ALP photon coupling. We exclude axion-photon couplings  $g_{a\gamma} > 3.9\text{--}7.8 \times 10^{-11} \text{ GeV}^{-1}$  at the 95% CL for  $m_a \lesssim 4 \times 10^{-7} \text{ eV}$ .

At this regard, we have evaluated the changes in the assumption we have done (e.g. the module of the magnetic field and the star formation rate model) finding a factor  $\sim 2$  of difference between the two extremal cases. Despite such a factor is not huge for an astrophysical bound, it changes the nature of our bound from being competitive with the benchmark CAST bound to being completely inside the CAST excluded region.

Of course with a better characterization of the strength of the magnetic fields in the host galaxies one would strengthen the robustness of the bound.

Finally, we remark that a significant part of ALP parameter space is left open to future gamma-ray experiments like CTA,

as well as for forthcoming ALP searches, e.g. with ALPS-II [112] and IAXO [113] experiments. Therefore, exciting times have to be expected in ALP searches due to the unprecedented sensitivity of future gamma-ray and axion experiments that will start soon.

**Acknowledgements** We thank Francesca Calore and Christopher Ecker for useful discussions. This work of M.C., G.M., A.M., D.M. was partially supported by the research grant number 2017W4HA7S “NAT-NET: Neutrino and Astroparticle Theory Network” under the program PRIN 2017 funded by the Italian Ministero dell’Università e della Ricerca (MUR). The authors also acknowledge the support by the research project TAsP (Theoretical Astroparticle Physics) funded by the Istituto Nazionale di Fisica Nucleare (INFN).

The work of P.C. is supported by the European Research Council under Grant No. 742104 and by the Swedish Research Council (VR) under Grants 2018-03641 and 2019-02337. The work of L.M. is supported by the Italian Istituto Nazionale di Fisica Nucleare (INFN) through the “QGSKY” project and by Ministero dell’Istruzione, Università e Ricerca (MIUR). The work of D.F.G.F. is partially supported by the VILLUM FONDEN under project no. 29388. This project has received funding from the European Union’s Horizon 2020 research and innovation program under the Marie Skłodowska-Curie grant agreement No. 847523 ‘INTERACTIONS’. The computational work has been executed on the IT resources of the ReCaS-Bari data center, which have been made available by two projects financed by the MIUR (Italian Ministry for Education, University and Research) in the “PON Ricerca e Competitività 2007-2013” Program: ReCaS (Azione I-Interventi di rafforzamento strutturale, PONa3\_00052, Avviso 254/Ric) and PRISMA (Asse II-Sostegno all’innovazione, PON04a2A).

**Data Availability Statement** This manuscript has no associated data or the data will not be deposited. [Authors’ comment: Data sharing is not applicable to this article as no datasets were generated or analysed during the current study.]

**Open Access** This article is licensed under a Creative Commons Attribution 4.0 International License, which permits use, sharing, adaptation, distribution and reproduction in any medium or format, as long as you give appropriate credit to the original author(s) and the source, provide a link to the Creative Commons licence, and indicate if changes were made. The images or other third party material in this article are included in the article’s Creative Commons licence, unless indicated otherwise in a credit line to the material. If material is not included in the article’s Creative Commons licence and your intended use is not permitted by statutory regulation or exceeds the permitted use, you will need to obtain permission directly from the copyright holder. To view a copy of this licence, visit <http://creativecommons.org/licenses/by/4.0/>.

Funded by SCOAP<sup>3</sup>. SCOAP<sup>3</sup> supports the goals of the International Year of Basic Sciences for Sustainable Development.

## Appendix A: Systematic uncertainty on the LHAASO upper limits on $g_{a\gamma}$

In this Appendix we comment about the systematic uncertainty on the LHAASO upper limits on  $g_{a\gamma}$  due to the different assumptions of our work. We take as benchmark case the host galaxy magnetic field as a single box with  $\langle |\mathbf{B}_T| \rangle = 5 \mu\text{G}$ , and the Fiducial case for neutrino fluxes in Table 1.

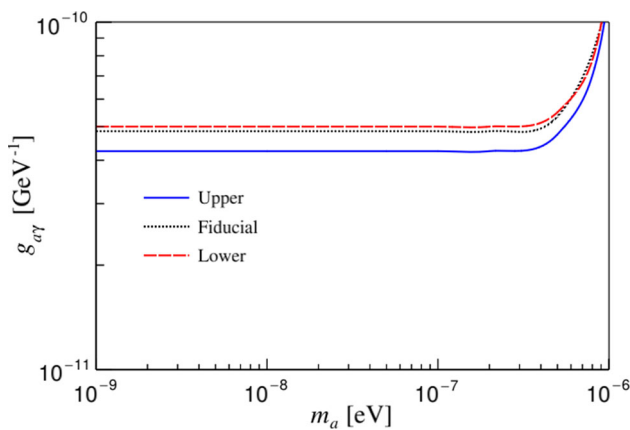


**Fig. 11** Variation in the bound on  $g_{a\gamma}$  in dependence of the initial fluxes described in Table 1: Upper (blue continuous curve), Fiducial (black dotted curve) and Lower (red dashed curve)

### A Impact of star formation rate and original photon spectrum models

We discuss the changes in the results obtained for the benchmark case, considering the Upper and Lower case in Table 1. These cases differ for the  $n_s$  and  $Q_\gamma$  models as described in the table. In Fig. 11 we show the difference in the constraints varying between the Lower, Fiducial and Upper case. As it is possible to see the bound is rather stable (there is only correction of  $\sim 10\%$ ). This is because the ALP flux strongly depends on  $g_{a\gamma}$  (in the perturbative regime it depends on  $g_{a\gamma}^4$ ).

### B Impact of host galaxy magnetic field

In Fig. 12 we show the impact on the exclusion plot for the benchmark case on the assumption of the magnetic field in the host galaxy. The continuous curve refers to the box model, while the dashed curve corresponds to the cell model. In each case the spread of the bound represents the variation of  $B_T \in [2, 8] \times 10^{-6}$  G. The red curves shown the minimum constraints obtained for  $B_T = 2 \mu\text{G}$ , while the black curves are for the maximum constraints obtained for  $B_T = 5 \mu\text{G}$  for the box model and  $B_T = 8 \mu\text{G}$  for the cell model. It results that the impact on the variation of the host galaxy magnetic field model is a factor  $\sim 1.5$  for both models.

### C Impact of photon background

Here we discuss how the bound changes if we assume the presence of an additional gamma-ray flux background in the Milky-Way. In this case the  $\gamma$ -ray flux on Earth can be written

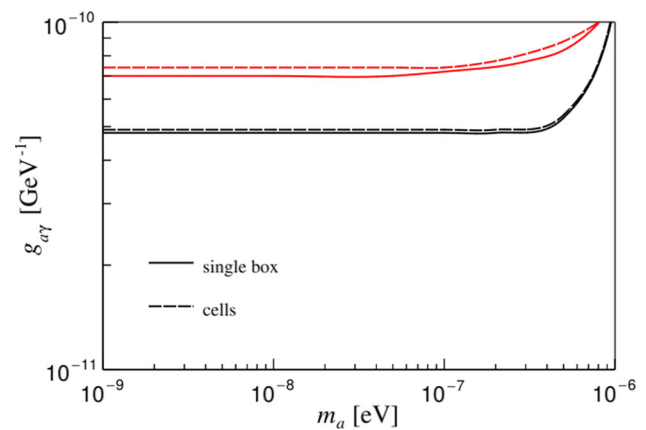


**Fig. 12** Variation in the bound due to the different choice of the magnetic field in the host galaxy. The continuous curve refers to the box model, while the dashed curve corresponds to the cell model while the black curves refer the maximum bound obtained in each model and the red curves refer to the minimum bound. In each case the spread of the bound represents the variation of  $B_T \in [2 : 8] \times 10^{-6}$  G

as:

$$\frac{d\phi_{\gamma,\oplus}}{dE} = P_{a\gamma}^{\text{MW}} \frac{d\phi_a}{dE} + \frac{d\phi_\gamma^{\text{bkg}}}{dE}, \quad (27)$$

where  $d\phi_\gamma^{\text{bkg}}/dE$  is the background photon flux. We model this background flux as a power-law:

$$\frac{d\phi_\gamma^{\text{bkg}}}{dE} = NE^\alpha \times F(E), \quad (28)$$

where  $N$  and  $\alpha$  are the two parameters of the power-law that have to be fitted and  $F(E_\gamma)$  is a reduction factor caused by the CMB and SL+Infrared absorption. The chosen background seems to properly fit into a  $2\sigma$  range all the points of the LHAASO data set except the last one. Therefore in our analysis, we focus only on the first eight experimental points. The reason is that, since we want to constrain an additional component to be added on top of this background, the results would not be reliable if the background itself were not realistic. We emphasize that eliminating one of the experimental points from our analysis is only conservative, since we are renouncing part of the information to constrain the model, and therefore the constraints we will draw are more robust.

In Fig. 13, we show the result from the fit without considering the presence of ALPs, obtaining a  $\chi_0^2 = 10.97$  over 6 degrees of freedom.

When the ALP flux is added on top of the background component, we find that the fit always worsens. Therefore, we consider the solution without ALP as the best fit over the combined parameter space of the background and the ALP flux. Using as a test statistic  $\chi^2 - \chi_0^2$ , and again accounting only for the upper fluctuations of the chi-squared, we exclude at



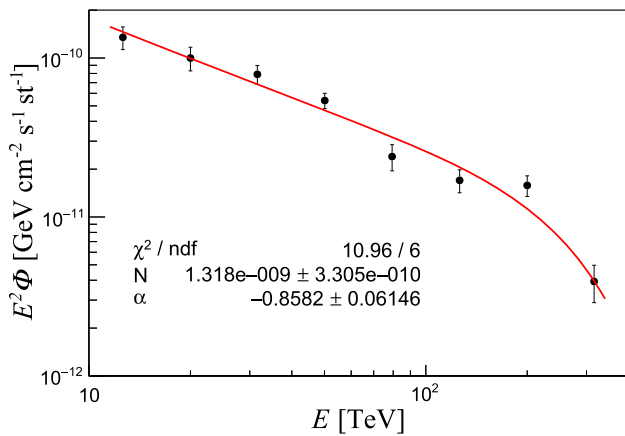


**Fig. 13** Fit of the LHAASO data points with the power-law background in Eq. (28). The  $\chi^2 \simeq 11$ , showing how it is only a fit acceptable into  $2\sigma$  errors

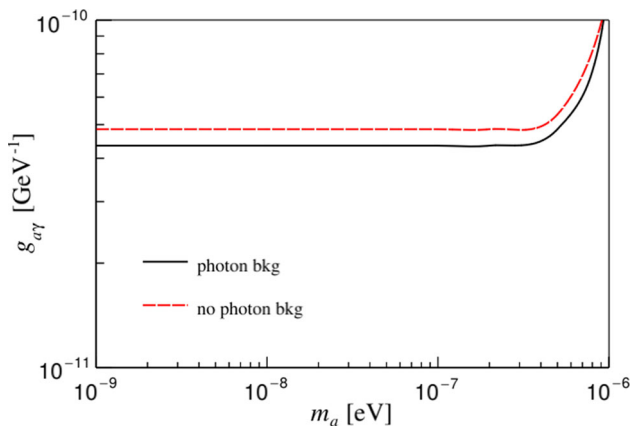


**Fig. 14** Impact on the constraint from the Fiducial case in the presence of a photon background. The case with no photon background in red dashed curve, while in the presence of a photon background we obtain the black curve

95% confidence level values of  $g_{a\gamma}$  such that  $\chi^2 - \chi_0^2 > 2.71$ . Due to the high value of  $\chi_0^2$ , denoting no correct background assumption, and to the strong dependence of the axion flux on  $g_{a\gamma}$ , there is some  $\mathcal{O}(10)$  % of difference with respect to the case without photon background as shown in Fig. 14.

**References**

1. P. Svrcek, E. Witten, Axions in string theory. *JHEP* **06**, 051 (2006). <https://doi.org/10.1088/1126-6708/2006/06/051>. [arXiv:hep-th/0605206](https://arxiv.org/abs/hep-th/0605206)
2. A. Arvanitaki, S. Dimopoulos, S. Dubovsky, N. Kaloper, J. March-Russell, String axiverse. *Phys. Rev. D* **81**, 123530 (2010). <https://doi.org/10.1103/PhysRevD.81.123530>. [arXiv:0905.4720](https://arxiv.org/abs/0905.4720) [hep-th]
3. M. Cicoli, M. Goodsell, A. Ringwald, The type IIB string axiverse and its low-energy phenomenology. *JHEP* **10**, 146 (2012). [https://doi.org/10.1007/JHEP10\(2012\)146](https://doi.org/10.1007/JHEP10(2012)146). [arXiv:1206.0819](https://arxiv.org/abs/1206.0819) [hep-th]

4. P.W. Graham, D.E. Kaplan, S. Rajendran, Cosmological relaxation of the electroweak scale. *Phys. Rev. Lett.* **115**, 221801 (2015). <https://doi.org/10.1103/PhysRevLett.115.221801>. [arXiv:1504.07551](https://arxiv.org/abs/1504.07551) [hep-ph]
5. L. Di Luzio, M. Giannotti, E. Nardi, L. Visinelli, The landscape of QCD axion models. *Phys. Rep.* **870**, 1–117 (2020). <https://doi.org/10.1016/j.physrep.2020.06.002>. [arXiv:2003.01100](https://arxiv.org/abs/2003.01100) [hep-ph]
6. G. Raffelt, L. Stodolsky, Mixing of the photon with low mass particles. *Phys. Rev. D* **37**, 1237 (1988). <https://doi.org/10.1103/PhysRevD.37.1237>
7. A.A. Anselm, Experimental test for arion  $\leftrightarrow$  photon oscillations in a homogeneous constant magnetic field. *Phys. Rev. D* **37**, 2001 (1988). <https://doi.org/10.1103/PhysRevD.37.2001>
8. P.W. Graham, I.G. Irastorza, S.K. Lamoreaux, A. Lindner, K.A. van Bibber, Experimental searches for the axion and axion-like particles. *Ann. Rev. Nucl. Part. Sci.* **65**, 485–514 (2015). <https://doi.org/10.1146/annurev-nucl-102014-022120>. [arXiv:1602.00039](https://arxiv.org/abs/1602.00039) [hep-ex]
9. I.G. Irastorza, J. Redondo, New experimental approaches in the search for axion-like particles. *Prog. Part. Nucl. Phys.* **102**, 89–159 (2018). <https://doi.org/10.1016/j.ppnp.2018.05.003>. [arXiv:1801.08127](https://arxiv.org/abs/1801.08127) [hep-ph]
10. I.G. Irastorza, An introduction to axions and their detection, in *Les Houches Summer School on Dark Matter* (2021) <https://doi.org/10.21468/SciPostPhysLectNotes.45>. [arXiv:2109.07376](https://arxiv.org/abs/2109.07376) [hep-ph]
11. P. Sikivie, Invisible axion search methods. *Rev. Mod. Phys.* **93**, 015004 (2021). <https://doi.org/10.1103/RevModPhys.93.015004>. [arXiv:2003.02206](https://arxiv.org/abs/2003.02206) [hep-ph]
12. A. Mirizzi, G.G. Raffelt, P.D. Serpico, Signatures of axion-like particles in the spectra of TeV gamma-ray sources. *Phys. Rev. D* **76**, 023001 (2007). <https://doi.org/10.1103/PhysRevD.76.023001>. [arXiv:0704.3044](https://arxiv.org/abs/0704.3044) [astro-ph]
13. A. De Angelis, O. Mansutti, M. Roncadelli, Axion-like particles, cosmic magnetic fields and gamma-ray astrophysics. *Phys. Lett. B* **659**, 847–855 (2008). <https://doi.org/10.1016/j.physletb.2007.12.012>. [arXiv:0707.2695](https://arxiv.org/abs/0707.2695) [astro-ph]
14. A. De Angelis, M. Roncadelli, O. Mansutti, Evidence for a new light spin-zero boson from cosmological gamma-ray propagation? *Phys. Rev. D* **76**, 121301 (2007). <https://doi.org/10.1103/PhysRevD.76.121301>. [arXiv:0707.4312](https://arxiv.org/abs/0707.4312) [astro-ph]
15. D. Hooper, P.D. Serpico, Detecting axion-like particles with gamma ray telescopes. *Phys. Rev. Lett.* **99**, 231102 (2007). <https://doi.org/10.1103/PhysRevLett.99.231102>. [arXiv:0706.3203](https://arxiv.org/abs/0706.3203) [hep-ph]
16. M. Simet, D. Hooper, P.D. Serpico, The Milky Way as a kiloparsec-scale axionscope. *Phys. Rev. D* **77**, 063001 (2008). <https://doi.org/10.1103/PhysRevD.77.063001>. [arXiv:0712.2825](https://arxiv.org/abs/0712.2825) [astro-ph]
17. A. De Angelis, G. Galanti, M. Roncadelli, Relevance of axion-like particles for very-high-energy astrophysics. *Phys. Rev. D* **84**, 105030 (2011) [Erratum: *Phys.Rev.D* **87**, 109903 (2013)]. <https://doi.org/10.1103/PhysRevD.84.105030>. [arXiv:1106.1132](https://arxiv.org/abs/1106.1132) [astro-ph.HE]
18. A. Mirizzi, D. Montanino, Stochastic conversions of TeV photons into axion-like particles in extragalactic magnetic fields. *JCAP* **12**, 004 (2009). <https://doi.org/10.1088/1475-7516/2009/12/004>. [arXiv:0911.0015](https://arxiv.org/abs/0911.0015) [astro-ph.HE]
19. D. Horns, L. Maccione, M. Meyer, A. Mirizzi, D. Montanino, M. Roncadelli, Hardening of TeV gamma spectrum of AGNs in galaxy clusters by conversions of photons into axion-like particles. *Phys. Rev. D* **86**, 075024 (2012). <https://doi.org/10.1103/PhysRevD.86.075024>. [arXiv:1207.0776](https://arxiv.org/abs/1207.0776) [astro-ph.HE]
20. M. Meyer, D. Horns, M. Raue, First lower limits on the photon-axion-like particle coupling from very high energy gamma-ray observations. *Phys. Rev. D* **87**, 035027 (2013). <https://doi.org/10.1103/PhysRevD.87.035027>. [arXiv:1302.1208](https://arxiv.org/abs/1302.1208) [astro-ph.HE]

21. A. Abramowski et al. ( H.E.S.S.), Constraints on axionlike particles with H.E.S.S. from the irregularity of the PKS 2155-304 energy spectrum. *Phys. Rev. D* **88**, 102003 (2013). <https://doi.org/10.1103/PhysRevD.88.102003>. arXiv:1311.3148 [astro-ph.HE]
22. M. Meyer, D. Montanino, J. Conrad, On detecting oscillations of gamma rays into axion-like particles in turbulent and coherent magnetic fields. *JCAP* **09**, 003 (2014). <https://doi.org/10.1088/1475-7516/2014/09/003>. arXiv:1406.5972 [astro-ph.HE]
23. M. Meyer, J. Conrad, Sensitivity of the Cherenkov telescope array to the detection of axion-like particles at high gamma-ray opacities. *JCAP* **12**, 016 (2014). <https://doi.org/10.1088/1475-7516/2014/12/016>. arXiv:1410.1556 [astro-ph.HE]
24. M. Ajello et al., ( Fermi-LAT), Search for spectral irregularities due to photon-axionlike-particle oscillations with the fermi large area telescope. *Phys. Rev. Lett.* **116**, 161101 (2016). <https://doi.org/10.1103/PhysRevLett.116.161101>. arXiv:1603.06978 [astro-ph.HE]
25. D. Montanino, F. Vazza, A. Mirizzi, M. Viel, Enhancing the spectral hardening of cosmic TeV photons by mixing with axion-like particles in the magnetized cosmic web. *Phys. Rev. Lett.* **119**, 101101 (2017). <https://doi.org/10.1103/PhysRevLett.119.101101>. arXiv:1703.07314 [astro-ph.HE]
26. C. Zhang, Y.-F. Liang, S. Li, N.-H. Liao, L. Feng, Q. Yuan, Y.-Z. Fan, Z.-Z. Ren, New bounds on axionlike particles from the Fermi Large Area Telescope observation of PKS 2155–304. *Phys. Rev. D* **97**, 063009 (2018). <https://doi.org/10.1103/PhysRevD.97.063009>. arXiv:1802.08420 [hep-ph]
27. Z.-Q. Xia, C. Zhang, Y.-F. Liang, L. Feng, Q. Yuan, Y.-Z. Fan, W. Jian, Searching for spectral oscillations due to photon-axionlike particle conversion using the Fermi-LAT observations of bright supernova remnants. *Phys. Rev. D* **97**, 063003 (2018). <https://doi.org/10.1103/PhysRevD.97.063003>. arXiv:1801.01646 [astro-ph.HE]
28. J. Majumdar, F. Calore, D. Horns, Search for gamma-ray spectral modulations in Galactic pulsars. *JCAP* **04**, 048 (2018). <https://doi.org/10.1088/1475-7516/2018/04/048>. arXiv:1801.08813 [hep-ph]
29. G. Galanti, F. Tavecchio, M. Roncadelli, C. Evoli, Blazar VHE spectral alterations induced by photon-ALP oscillations. *Mon. Not. R. Astron. Soc.* **487**, 123–132 (2019). <https://doi.org/10.1093/mnras/stz1144>. arXiv:1811.03548 [astro-ph.HE]
30. Y.-F. Liang, C. Zhang, Z.-Q. Xia, L. Feng, Q. Yuan, Y.-Z. Fan, Constraints on axion-like particle properties with TeV gamma-ray observations of Galactic sources. *JCAP* **06**, 042 (2019). <https://doi.org/10.1088/1475-7516/2019/06/042>. arXiv:1804.07186 [hep-ph]
31. J. Bu, Y.-P. Li, Constraints on axionlike particles with different magnetic field models from the PKS 2155-304 energy spectrum. (2019). <https://doi.org/10.1088/1674-4527/19/10/154>. arXiv:1906.00357 [astro-ph.HE]
32. J.-G. Cheng, Y.-J. He, Y.-F. Liang, R.-J. Lu, E.-W. Liang, Revisiting the analysis of axion-like particles with the Fermi-LAT gamma-ray observation of NGC1275. (2020). arXiv:2010.12396 [astro-ph.HE]
33. P. Carena, C. Evoli, M. Giannotti, A. Mirizzi, D. Montanino, Turbulent axion-photon conversions in the Milky Way. *Phys. Rev. D* **104**, 023003 (2021). <https://doi.org/10.1103/PhysRevD.104.023003>. arXiv:2104.13935 [hep-ph]
34. M.C. David Marsh, J.H. Matthews, C. Reynolds, P. Carena, The Fourier formalism for relativistic axion-photon conversion, with astrophysical applications. (2021). arXiv:2107.08040 [hep-ph]
35. J.S. Reynés, J.H. Matthews, C.S. Reynolds, H.R. Russell, R.N. Smith, M.C. David Marsh, New constraints on light axion-like particles using Chandra transmission grating spectroscopy of the powerful cluster-hosted quasar H1821+643. *Mon. Not. R. Astron. Soc.* **510**, 1264–1277 (2021). <https://doi.org/10.1093/mnras/stab3464>. arXiv:2109.03261 [astro-ph.HE]
36. J.H. Matthews, C.S. Reynolds, M.C. David Marsh, J. Sisk-Reynés, P.E. Rodman, How do magnetic field models affect astrophysical limits on light axion-like particles? An X-ray case study with NGC 1275. *Astrophys. J.* **930**, 90 (2022). <https://doi.org/10.3847/1538-4357/ac5625>. arXiv:2202.08875 [astro-ph.HE]
37. S. Jacobsen, T. Linden, K. Freese, Constraining axion-like particles with HAWC observations of TeV blazars. (2022). arXiv:2203.04332 [hep-ph]
38. G. Galanti, M. Roncadelli, Axion-like particles implications for high-energy astrophysics. *Universe* **8**, 253 (2022). <https://doi.org/10.3390/universe8050253>. arXiv:2205.00940 [hep-ph]
39. M.G. Aartsen et al., (IceCube), First observation of PeV-energy neutrinos with IceCube. *Phys. Rev. Lett.* **111**, 021103 (2013). <https://doi.org/10.1103/PhysRevLett.111.021103>. arXiv:1304.5356 [astro-ph.HE]
40. M.G. Aartsen et al. (IceCube), Evidence for high-energy extraterrestrial neutrinos at the IceCube detector. *Science* **342**, 1242856 (2013). <https://doi.org/10.1126/science.1242856>. arXiv:1311.5238 [astro-ph.HE]
41. M.G. Aartsen et al., (IceCube), Observation of high-energy astrophysical neutrinos in three years of IceCube data. *Phys. Rev. Lett.* **113**, 101101 (2014). <https://doi.org/10.1103/PhysRevLett.113.101101>. arXiv:1405.5303 [astro-ph.HE]
42. M.G. Aartsen et al., (IceCube), Evidence for Astrophysical Muon Neutrinos from the Northern Sky with IceCube. *Phys. Rev. Lett.* **115**, 081102 (2015). <https://doi.org/10.1103/PhysRevLett.115.081102>. arXiv:1507.04005 [astro-ph.HE]
43. M.G. Aartsen et al. (IceCube), Observation and characterization of a cosmic muon neutrino flux from the northern hemisphere using six years of IceCube data. *Astrophys. J.* **833**, 3 (2016). <https://doi.org/10.3847/0004-637X/833/1/3>. arXiv:1607.08006 [astro-ph.HE]
44. M. Ahlers, F. Halzen, Opening a New Window onto the Universe with IceCube. *Prog. Part. Nucl. Phys.* **102**, 73–88 (2018). <https://doi.org/10.1016/j.pnpnp.2018.05.001>. arXiv:1805.11112 [astro-ph.HE]
45. R. Abbasi et al. (IceCube), The IceCube high-energy starting event sample: description and flux characterization with 7.5 years of data. *Phys. Rev. D* **104**, 022002 (2021). <https://doi.org/10.1103/PhysRevD.104.022002>. arXiv:2011.03545 [astro-ph.HE]
46. H. Vogel, R. Laha, M. Meyer, Diffuse axion-like particle searches. *PoS NOW2018*, 091 (2019). <https://doi.org/10.22323/1.337.0091>. arXiv:1712.01839 [hep-ph]
47. C. Eckner, F. Calore, First constraints on axion-like particles from Galactic sub-PeV gamma rays. (2022). arXiv:2204.12487 [astro-ph.HE]
48. A. Addazi et al. (LHAASO), The Large High Altitude Air Shower Observatory (LHAASO) Science Book (2021 Edition). *Chin. Phys. C* **46**, 035001–035007 (2022). arXiv:1905.02773 [astro-ph.HE]
49. S. Zhao, R. Zhang, Y. Zhang, Q. Yuan (LHAASO), Measurement of the diffuse gamma-ray emission from Galactic plane with LHAASO-KM2A. *PoS ICRC2021*, 859 (2021). <https://doi.org/10.22323/1.395.0859>
50. K. Murase, D. Guetta, M. Ahlers, Hidden cosmic-ray accelerators as an origin of TeV–PeV cosmic neutrinos. *Phys. Rev. Lett.* **116**, 071101 (2016). <https://doi.org/10.1103/PhysRevLett.116.071101>. arXiv:1509.00805 [astro-ph.HE]
51. A. Capanema, A. Esmaili, K. Murase, New constraints on the origin of medium-energy neutrinos observed by IceCube. *Phys. Rev. D* **101**, 103012 (2020). <https://doi.org/10.1103/PhysRevD.101.103012>. arXiv:2002.07192 [hep-ph]
52. A. Capanema, A. Esmaili, P.D. Serpico, Where do IceCube neutrinos come from? Hints from the diffuse gamma-ray flux. *JCAP*

- 02, 037 (2021). <https://doi.org/10.1088/1475-7516/2021/02/037>. arXiv:2007.07911 [hep-ph]
53. A. Loeb, E. Waxman, The cumulative background of high energy neutrinos from starburst galaxies. *JCAP* **05**, 003 (2006). <https://doi.org/10.1088/1475-7516/2006/05/003>. arXiv:astro-ph/0601695
  54. T.A. Thompson, E. Quataert, E. Waxman, A. Loeb, Assessing the starburst contribution to the gamma-ray and neutrino backgrounds. (2006). arXiv:astro-ph/0608699
  55. I. Tamborra, S. Ando, K. Murase, Star-forming galaxies as the origin of diffuse high-energy backgrounds: Gamma-ray and neutrino connections, and implications for starburst history. *JCAP* **09**, 043 (2014). <https://doi.org/10.1088/1475-7516/2014/09/043>. arXiv:1404.1189 [astro-ph.HE]
  56. X.-C. Chang, X.-Y. Wang, The diffuse gamma-ray flux associated with sub-PeV/PeV neutrinos from starburst galaxies. *Astrophys. J.* **793**, 131 (2014). <https://doi.org/10.1088/0004-637X/793/2/131>. arXiv:1406.1099 [astro-ph.HE]
  57. N. Senno, P. Mészáros, K. Murase, P. Baerwald, M.J. Rees, Extragalactic star-forming galaxies with hypernovae and supernovae as high-energy neutrino and gamma-ray sources: the case of the 10 TeV neutrino data. *Astrophys. J.* **806**, 24 (2015). <https://doi.org/10.1088/0004-637X/806/1/24>. arXiv:1501.04934 [astro-ph.HE]
  58. S. Chakraborty, I. Izaguirre, Diffuse neutrinos from extragalactic supernova remnants: dominating the 100 TeV IceCube flux. *Phys. Lett. B* **745**, 35–39 (2015). <https://doi.org/10.1016/j.physletb.2015.04.032>. arXiv:1501.02615 [hep-ph]
  59. E. Peretti, P. Blasi, F. Aharonian, G. Morlino, Cosmic ray transport and radiative processes in nuclei of starburst galaxies. *Mon. Not. R. Astron. Soc.* **487**, 168–180 (2019). <https://doi.org/10.1093/mnras/stz1161>. arXiv:1812.01996 [astro-ph.HE]
  60. E. Peretti, P. Blasi, F. Aharonian, G. Morlino, P. Cristofari, Contribution of starburst nuclei to the diffuse gamma-ray and neutrino flux. *Mon. Not. R. Astron. Soc.* **493**, 5880–5891 (2020). <https://doi.org/10.1093/mnras/staa698>. arXiv:1911.06163 [astro-ph.HE]
  61. A. Ambrosone, M. Chianese, D.F.G. Fiorillo, A. Marinelli, G. Miele, O. Pisanti, Starburst galaxies strike back: a multi-messenger analysis with Fermi-LAT and IceCube data. *Mon. Not. R. Astron. Soc.* **503**, 4032–4049 (2021). <https://doi.org/10.1093/mnras/stab659>. arXiv:2011.02483 [astro-ph.HE]
  62. A. Ambrosone, M. Chianese, D.F.G. Fiorillo, A. Marinelli, G. Miele, Could nearby star-forming galaxies light up the pointlike neutrino sky? *Astrophys. J. Lett.* **919**, L32 (2021). <https://doi.org/10.3847/2041-8213/ac25ff>. arXiv:2106.13248 [astro-ph.HE]
  63. F.W. Stecker, M.H. Salamon, High-energy neutrinos from quasars. *Space Sci. Rev.* **75**, 341–355 (1996). <https://doi.org/10.1007/BF00195044>. arXiv:astro-ph/9501064
  64. A. Atayan, C.D. Dermer, High-energy neutrinos from photomeson processes in blazars. *Phys. Rev. Lett.* **87**, 221102 (2001). <https://doi.org/10.1103/PhysRevLett.87.221102>. arXiv:astro-ph/0108053
  65. K. Murase, Y. Inoue, C.D. Dermer, Diffuse neutrino intensity from the inner jets of active galactic nuclei: impacts of external photon fields and the blazar sequence. *Phys. Rev. D* **90**, 023007 (2014). <https://doi.org/10.1103/PhysRevD.90.023007>. arXiv:1403.4089 [astro-ph.HE]
  66. P. Padovani, E. Resconi, P. Giommi, B. Arsioli, Y.L. Chang, Extreme blazars as counterparts of IceCube astrophysical neutrinos. *Mon. Not. R. Astron. Soc.* **457**, 3582–3592 (2016). <https://doi.org/10.1093/mnras/stw228>. arXiv:1601.06550 [astro-ph.HE]
  67. J. Alvarez-Muniz, P. Meszaros, High energy neutrinos from radio-quiet AGNs. *Phys. Rev. D* **70**, 123001 (2004). <https://doi.org/10.1103/PhysRevD.70.123001>. arXiv:astro-ph/0409034
  68. A. Pe'er, K. Murase, P. Meszaros, Radio quiet AGNs as possible sources of ultra-high energy cosmic rays. *Phys. Rev. D* **80**, 123018 (2009). <https://doi.org/10.1103/PhysRevD.80.123018>. arXiv:0911.1776 [astro-ph.HE]
  69. A. Palladino, X. Rodrigues, S. Gao, W. Winter, Interpretation of the diffuse astrophysical neutrino flux in terms of the blazar sequence. *Astrophys. J.* **871**, 41 (2019). <https://doi.org/10.3847/1538-4357/aaf507>. arXiv:1806.04769 [astro-ph.HE]
  70. B. Paczynski, G.H. Xu, Neutrino bursts from gamma-ray bursts. *Astrophys. J.* **427**, 708–713 (1994). <https://doi.org/10.1086/174178>
  71. E. Waxman, J.N. Bahcall, High-energy neutrinos from cosmological gamma-ray burst fireballs. *Phys. Rev. Lett.* **78**, 2292–2295 (1997). <https://doi.org/10.1103/PhysRevLett.78.2292>. arXiv:astro-ph/9701231
  72. K. Murase, S. Nagataki, High energy neutrino emission and neutrino background from gamma-ray bursts in the internal shock model. *Phys. Rev. D* **73**, 063002 (2006). <https://doi.org/10.1103/PhysRevD.73.063002>. arXiv:astro-ph/0512275
  73. P. Baerwald, S. Hummer, W. Winter, Magnetic field and flavor effects on the gamma-ray burst neutrino flux. *Phys. Rev. D* **83**, 067303 (2011). <https://doi.org/10.1103/PhysRevD.83.067303>. arXiv:1009.4010 [astro-ph.HE]
  74. M. Bustamante, K. Murase, W. Winter, J. Heinze, Multimessenger light curves from gamma-ray bursts in the internal shock model. *Astrophys. J.* **837**, 33 (2017). <https://doi.org/10.3847/1538-4357/837/1/33>. arXiv:1606.02325 [astro-ph.HE]
  75. R. Abbasi et al. (IceCube), Improved characterization of the astrophysical muon-neutrino flux with 9.5 years of IceCube data. *Astrophys. J.* **928**, 50 (2022). <https://doi.org/10.3847/1538-4357/ac4d29>. arXiv:2111.10299 [astro-ph.HE]
  76. M.G. Aartsen et al., (IceCube), Characteristics of the diffuse astrophysical electron and tau neutrino flux with six years of IceCube high energy cascade data. *Phys. Rev. Lett.* **125**, 121104 (2020). <https://doi.org/10.1103/PhysRevLett.125.121104>. arXiv:2001.09520 [astro-ph.HE]
  77. R. Abbasi et al. (IceCube), The IceCube high-energy starting event sample: description and flux characterization with 7.5 years of data. (2020). arXiv:2011.03545 [astro-ph.HE]
  78. H. Yuksel, M.D. Kistler, J.F. Beacom, A.M. Hopkins, Revealing the high-redshift star formation rate with gamma-ray bursts. *Astrophys. J. Lett.* **683**, L5–L8 (2008). <https://doi.org/10.1086/591449>. arXiv:0804.4008 [astro-ph]
  79. S. Horiuchi, J.F. Beacom, E. Dwek, The diffuse supernova neutrino background is detectable in super-Kamiokande. *Phys. Rev. D* **79**, 083013 (2009). <https://doi.org/10.1103/PhysRevD.79.083013>. arXiv:0812.3157 [astro-ph]
  80. F. Halzen, A. Kheirandish, T. Weisgarber, S.P. Wakely, On the neutrino flares from the direction of TXS 0506+056. *Astrophys. J. Lett.* **874**, L9 (2019). <https://doi.org/10.3847/2041-8213/ab0d27>. arXiv:1811.07439 [astro-ph.HE]
  81. A. Kartavtsev, G. Raffelt, H. Vogel, Extragalactic photon-ALP conversion at CTA energies. *JCAP* **01**, 024 (2017). <https://doi.org/10.1088/1475-7516/2017/01/024>. arXiv:1611.04526 [astro-ph.HE]
  82. A. Mirizzi, G.G. Raffelt, P.D. Serpico, Photon-axion conversion as a mechanism for supernova dimming: limits from CMB spectral distortion. *Phys. Rev. D* **72**, 023501 (2005). <https://doi.org/10.1103/PhysRevD.72.023501>. arXiv:astro-ph/0506078
  83. A. Mirizzi, G.G. Raffelt, P.D. Serpico, Photon-axion conversion in intergalactic magnetic fields and cosmological consequences. *Lect. Notes Phys.* **741**, 115–134 (2008). [https://doi.org/10.1007/978-3-540-73518-2\\_7](https://doi.org/10.1007/978-3-540-73518-2_7). arXiv:astro-ph/0607415
  84. A. Dobrynina, A. Kartavtsev, G. Raffelt, Photon-photon dispersion of TeV gamma rays and its role for photon-ALP conversion. *Phys. Rev. D* **91**, 083003 (2015) [Erratum: *Phys. Rev. D* **95**, 109905 (2017)]. <https://doi.org/10.1103/PhysRevD.91.083003>. arXiv:1412.4777 [astro-ph.HE]



85. R.J. Gould, G.P. Schreder, Pair production in photon–photon collisions. *Phys. Rev.* **155**, 1404–1407 (1967) <https://doi.org/10.1103/PhysRev.155.1404>
86. W. Heitler, *The Quantum Theory of Radiation, International Series of Monographs on Physics*, vol. 5 (Oxford University Press, Oxford, 1936)
87. T.A. Porter, G. Johannesson, I.V. Moskalenko, High-energy gamma rays from the Milky Way: three-dimensional spatial models for the cosmic-ray and radiation field densities in the interstellar medium. *Astrophys. J.* **846**, 67 (2017). <https://doi.org/10.3847/1538-4357/aa844d>. arXiv:1708.00816 [astro-ph.HE]
88. D. Moss, A. Shukurov, Turbulence and magnetic fields in elliptical galaxies. *Mon. Not. R. Astron. Soc.* **279**, 229–239 (1996)
89. F. Tavecchio, M. Roncadelli, G. Galanti, G. Bonnoli, Evidence for an axion-like particle from PKS 1222+216? *Phys. Rev. D* **86**, 085036 (2012). <https://doi.org/10.1103/PhysRevD.86.085036>. arXiv:1202.6529 [astro-ph.HE]
90. A. Fletcher, Magnetic fields in nearby galaxies. *ASP Conf. Ser.* **438**, 197–210 (2011). arXiv:1104.2427 [astro-ph.CO]
91. R. Beck, R. Wielebinski, Magnetic fields in the Milky Way and in galaxies. (2013). [https://doi.org/10.1007/978-94-007-5612-0\\_13](https://doi.org/10.1007/978-94-007-5612-0_13). arXiv:1302.5663 [astro-ph.GA]
92. R. Pakmor, F.A. Gómez, R.J.J. Grand, F. Marinacci, C.M. Simpson, V. Springel, D. J.R. Campbell, C.S. Frenk, T. Guillet, C. Pfrommer, S.D.M. White, Magnetic field formation in the Milky Way like disc galaxies of the Auriga project. *Mon. Not. R. Astron. Soc.* **469**, 3185–3199 (2017). <https://doi.org/10.1093/mnras/stx1074>
93. N. Bassan, A. Mirizzi, M. Roncadelli, Axion-like particle effects on the polarization of cosmic high-energy gamma sources. *JCAP* **05**, 010 (2010). <https://doi.org/10.1088/1475-7516/2010/05/010>. arXiv:1001.5267 [astro-ph.HE]
94. M. Krause, Magnetic fields and halos in spiral galaxies. *Galaxies* **7** (2019). <https://doi.org/10.3390/galaxies7020054>
95. L.F.S. Rodrigues, L. Chamandy, A. Shukurov, C.M. Baugh, A.R. Taylor, Evolution of galactic magnetic fields. *Mon. Not. R. Astron. Soc.* **483**, 2424–2440 (2018). <https://doi.org/10.1093/mnras/sty3270>. <https://academic.oup.com/mnras/article-pdf/483/2/2424/27184716/sty3270.pdf>.
96. F.C. Adams, G. Laughlin, A dying universe: the long term fate and evolution of astrophysical objects. *Rev. Mod. Phys.* **69**, 337–372 (1997). <https://doi.org/10.1103/RevModPhys.69.337>. arXiv:astro-ph/9701131
97. R. Jansson, G.R. Farrar, A new model of the galactic magnetic field. *Astrophys. J.* **757**, 14 (2012). <https://doi.org/10.1088/0004-637X/757/1/14>. arXiv:1204.3662 [astro-ph.GA]
98. R. Adam et al. (Planck), Planck intermediate results.: XLII. Large-scale Galactic magnetic fields. *Astron. Astrophys.* **596**, A103 (2016). <https://doi.org/10.1051/0004-6361/201528033> arXiv:1601.00546 [astro-ph.GA]
99. J.M. Cordes, T.J.W. Lazio, NE2001. 1. A New model for the galactic distribution of free electrons and its fluctuations. (2002). arXiv:astro-ph/0207156
100. F. Calore, P. Carena, M. Giannotti, J. Jaeckel, A. Mirizzi, Bounds on axionlike particles from the diffuse supernova flux. *Phys. Rev. D* **102**, 123005 (2020). <https://doi.org/10.1103/PhysRevD.102.123005>. arXiv:2008.11741 [hep-ph]
101. V. Anastassopoulos et al., (CAST), New CAST limit on the axion-photon interaction. *Nat. Phys.* **13**, 584–590 (2017). <https://doi.org/10.1038/nphys4109>. arXiv:1705.02290 [hep-ex]
102. A. Ayala, I. Domínguez, M. Giannotti, A. Mirizzi, O. Straniero, Revisiting the bound on axion-photon coupling from globular clusters. *Phys. Rev. Lett.* **113**, 191302 (2014). <https://doi.org/10.1103/PhysRevLett.113.191302>. arXiv:1406.6053 [astro-ph.SR]
103. A. Payez, C. Evoli, T. Fischer, M. Giannotti, A. Mirizzi, A. Ringwald, Revisiting the SN1987A gamma-ray limit on ultralight axion-like particles. *JCAP* **02**, 006 (2015). <https://doi.org/10.1088/1475-7516/2015/02/006>. arXiv:1410.3747 [astro-ph.HE]
104. H.-J. Li, J.-G. Guo, X.-J. Bi, S.-J. Lin, P.-F. Yin, Limits on axion-like particles from Mrk 421 with 4.5-year period observations by ARGO-YBJ and Fermi-LAT. *Phys. Rev. D* **103**, 083003 (2021). <https://doi.org/10.1103/PhysRevD.103.083003>. arXiv:2008.09464 [astro-ph.HE]
105. G.A. Pallathadka, F. Calore, P. Carena, M. Giannotti, D. Horns, J. Majumdar, A. Mirizzi, A. Ringwald, A. Sokolov, F. Stief, Reconciling hints on axion-like-particles from high-energy gamma rays with stellar bounds. (2020), arXiv:2008.08100 [hep-ph]
106. M. Ajello et al., (Fermi-LAT), Search for spectral irregularities due to photon-axionlike-particle oscillations with the Fermi large area telescope. *Phys. Rev. Lett.* **116**, 161101 (2016). <https://doi.org/10.1103/PhysRevLett.116.161101>. arXiv:1603.06978 [astro-ph.HE]
107. A. Abramowski et al. (H.E.S.S.), Constraints on axionlike particles with H.E.S.S. from the irregularity of the PKS 2155-304 energy spectrum. *Phys. Rev. D* **88**, 102003 (2013). <https://doi.org/10.1103/PhysRevD.88.102003>. arXiv:1311.3148 [astro-ph.HE]
108. M. Libanov, S. Troitsky, On the impact of magnetic-field models in galaxy clusters on constraints on axion-like particles from the lack of irregularities in high-energy spectra of astrophysical sources. *Phys. Lett. B* **802**, 135252 (2020). <https://doi.org/10.1016/j.physletb.2020.135252>. arXiv:1908.03084 [astro-ph.HE]
109. P. De la Torre Luque, D. Gaggero, D. Grasso, O. Fornieri, K. Egberts, C. Steppa, C. Evoli, Galactic diffuse gamma rays meet the PeV frontier. (2022). arXiv:2203.15759 [astro-ph.HE]
110. H. Abdalla et al. (CTA), Sensitivity of the Cherenkov Telescope Array for probing cosmology and fundamental physics with gamma-ray propagation. *JCAP* **02**, 048 (2021). <https://doi.org/10.1088/1475-7516/2021/02/048>. arXiv:2010.01349 [astro-ph.HE]
111. C. Dessert, D. Dunsky, B.R. Safdi, Upper limit on the axion-photon coupling from magnetic white dwarf polarization. (2022). arXiv:2203.04319 [hep-ph]
112. R. Bähre, B. Döbrich, J. Dreyling-Eschweiler, S. Ghazaryan, R. Hodajeri et al., Any light particle search—technical design report. *JINST* **8**, T09001 (2013). <https://doi.org/10.1088/1748-0221/8/09/T09001>. arXiv:1302.5647 [physics.ins-det]
113. E. Armengaud et al., (IAXO), Physics potential of the International Axion Observatory (IAXO). *JCAP* **06**, 047 (2019). <https://doi.org/10.1088/1475-7516/2019/06/047>. arXiv:1904.09155 [hep-ph]